Haidar Mas'ud ALFANDA

THEORETICAL AND EXPERIMENTAL STUDIES ON ELECTRONIC SPECTRA OF QUINOLINE CARBOXALDEHYDE MOLECULES

M.S.
2014

FATİH UNIVERSITY

The Graduate School of Sciences and Engineering

Master of Science in
Physics

THEORETICAL AND EXPERIMENTAL STUDIES ON ELECTRONIC ABSORPTION SPECTRA OF QUINOLINE CARBOXALDEHYDE DERIVATIVES

by

Haidar Mas'ud ALFANDA

May 2014

THEORETICAL AND EXPERIMENTAL STUDIES ON ELECTRONIC SPECTRA OF QUINOLINE CARBOXALDEHYDE DERIVATIVES

by

Haidar Mas'ud ALFANDA

A thesis submitted to

the Graduate School of Sciences and Engineering

of

Fatih University

in partial fulfillment of the requirements for the degree of

Master of Science

in

Physics

May 2014
İstanbul, Turkey

APPROVAL PAGE

This is to certify that I have read this thesis written by Haidar Mas'ud ALFANDA and that in my opinion it is fully adequate, in scope and quality, as a thesis for the degree of Master of Science in Physics.

_____
Prof. Dr. Mustafa KUMRU
Thesis Supervisor

I certify that this thesis satisfies all the requirements as a thesis for the degree of Master of Science in Physics.

_____
Prof. Dr. Mustafa KUMRU
Head of Department

Examining Committee Members

Prof. Dr. Mustafa KUMRU _____

Assoc. Prof. Dr. Ahmet ALTUN _____

Assoc. Prof. Dr. Ramazan ÖZTÜRK _____

It is approved that this thesis has been written in compliance with the formatting rules laid down by the Graduate School of Sciences and Engineering.

_____
Assoc. Prof. Dr. Nurullah ARSLAN
Director

May 2014

THEORETICAL AND EXPERIMENTAL STUDIES ON ELECTRONIC SPECTRA OF QUINOLINE CARBOXALDEHYDE DERIVATIVES

Haidar Mas'ud ALFANDA

M.Sc Thesis – Physics
May 2014

Thesis Supervisor: Prof. Dr. Mustafa KUMRU

ABSTRACT

In this work, the experimental and theoretical electronic absorption spectra of quinoline carboxaldehyde (QC) derivatives were studied. QC has seven different positional isomers, Q-n-C, n=2-8 depending on the position of aldehyde group. The UV-vis absorption spectra of the molecules under investigation were examined in the range of 190-1100 nm using water as solvent. There are two rotomers for QC depending on the spatial orientation of C=O. Computational results identified the most stable rotomer as Rot1. The geometrical parameters of all seven isomers were obtained using Density functional theory (DFT) at 6-311++G(d,p)/B3LYP level of theory. Electonic properties such as excitation energy, absorption wavelength, oscillator strength and HOMO and LUMO energies were performed by time dependent density functional theory (TD-DFT) in gas-phase and solvated phase of water. Finally the simulated spectra show good agreement with observed spectra.

Keywords: Quinoline carboxhaldehyde, electronic spectra, DFT, TD-DFT, HOMO-LUMO, MESP.

KUİNOLİN KARBOKSALDEHİD TÜREVLERİNİN ELEKTRONİK SOĞURMA SPEKTRUMLARI ÜZERİNE TEORİK VE DENEYSEL ÇALIŞMALAR

Haidar Mas'ud ALFANDA

Yüksek Lisans Tezi – Fizik
Mayıs 2014

Tez Danışmanı: Prof. Dr. Mustafa KUMRU

ÖZ

Bu çalışmada, kuinolin karboksaldahid (QC) nin deneysel ve teorik soğurma elektronik spektrumları çalışılmıştır. QC, aldehyde gurubunun konumuna bağlı olarak {Q-n-C, n=2-8}; yedi farklı konum izomerine sahiptir. İncelenen moleküllerin UV-vis soğurma spektrumları 190-1100 nm aralığında ve su çözeltisinde incelenmiştir. C=O nun uzaydaki yönelimine bağlı olarak QC nin iki rotomeri vardır. Hesaplama sonuçları, en kararlı rotomerin Rot1 olduğunu belirlemiştir. Yedi izomerin de geometrik parametreleri, 6-311++G(d,p)/B3LYP teori seviyesinde Yoğunluk Fonksiyonu Teorisi (DFT) kullanılarak elde edilmiştir. HOMO ve LUMO enerjileri, titreşici şiddeti, soğurma dalgaboyu ve uyarma enerjileri gibi elektronik özellikler; gaz ve suda çözünmüş fazlarda, zamana bağlı Yoğunluk Fonksiyonu Teorisi (TD-DFT) kullanılarak hesaplanmıştır. Son olarak; teorik spektrumların deneysel spektrumlar ile tam bir uyum içinde oldukları gözlenmiştir.

Anahtar Kelimeler: Kuinolin Karboksaldehid, elektronic spektrUM, Yoğunluk Fonksiyonu Teorisi (DFT), zamana bağlı Yoğunluk Fonksiyonu Teorisi (TD-DFT), HOMO-LUMO, MESP.

To my respected parents, with love…

ACKNOWLEDGEMENT

All praise is for Allah, in whose Hand is the dominion of the heavens and the earth, Lord and Sustainer of the worlds. Peace, blessings and salutations be upon Muhammad, his family, his Companions and all those who follow in their footsteps until the Last Day. To proceed…

I wish to express my graditude to Prof. Mustafa KUMRU for his academic guidance throughout my master's programme. My deepest appreciation goes to Assoc. Prof. Ahmet ALTUN for his thoughtful insight and immense assistance he has shown to me in producing this thesis. This thesis would not have been possible without his support. I am also grateful to Assoc. Prof. Sadik GÜNER for his guidance in recording experimental data. I also thank Assoc. Prof. Serkan ÇALIŞKAN and Assoc. Prof. Levent SARI for their wonderful lectures during my course work. Special regards to my jury member Assoc. Prof. Ramazan ÖZTÜRK for his kind words of advice and conscious critics.

My deepest gratitude goes to my mother and father for their unflagging love and support throughout my life. I am everything because of you and the confidence you have build on me. I appreciate your patience during my long absence abroad. Many wonderful memories are result of wonderful companionship of Nigerian friends to whom I am eternally grateful.

This acknowledgement would be incomplete without mentioning research assistant Tayyibe BARDAKÇI who took the task of introducing me to GAUSSIAN programme. I would also like to mention research assistant Mustafa KOCADEMİR whom we performed all experiments together.

Lastly, I thank Kano State Goverment under the administration of Engr. (Dr.) Rabi'u Musa Kwankwaso for giving me the opportunity to come to Turkey for higher studies; you opened a box of dreams that might have never been possible for me! I sealed up by quoting Qur'an (10:10):

Their call therein will be, "Exalted are You, O Allah," and their greeting therein will be, "Peace." And the last of their call will be, "Praise to Allah, Lord of the worlds!"

TABLE OF CONTENTS

LIST OF TABLES

TABLE

LIST OF FIGURES

FIGURE

LIST OF SYMBOLS AND ABBREVIATIONS

SYMBOL/ABBREVIATION

ΔE	HOMO-LUMO energy gap
A	Absorbance
A	Electron affinity
a	Specific absoptivity
b	Path length
B3	Becke's three parameter
B-O	Born-Oppenheimer approximation
C	Concentration of absorbing sample
c	Speed of light
DFT	Density functional theory
E_{tot}	Total energy of a molecule
E_{XC}	Exchange correlation functional
f	Oscillator strength
FMOs	Frontier molecular orbitals
GGA	Generalised gradient approximation
h	planck's constant
HK	Hohenberg-Kohn theorem
HOMO	Higest occupied molecular orbital
I	Ionisation potential
KS	Kohn-Sham
LDA	Local density approximation
LUMO	Lowest unoccupied molecular orbital
LYP	Lee-Yang-Parr
MESP	Molecular electrostatic potential
MO	Molecular orbital
n	Unshared electrons

P	Transmitted radiation
P_0	Incident radiation
PCM	Polarisable continuum model
QC	Quinoline carboxaldehyde
T	Transmittance
TD-DFT	Time dependent Density functional theory
TF	Thomas-Fermi model
UV-vis	Ultraviolet visible Spectroscopy
ε	Molar extinction coefficient
ε_{HOMO}	Energy of HOMO
ε_{LUMO}	Energy of LUMO
η	Chemical hardness
λ	Wavelength
μ	Chemical potential
π	Pi orbital
ρ(**r**)	Electron density
σ	Sigma orbital
υ	Photon frequency
χ	Electronegativity
ψ_r	Rotational wave function
ψ_{total}	Total molecular wave function
ψ_υ	Vibrational wave function
ω	Electrophilicity index

CHAPTER 1

INTRODUCTION

Quinoline is a heterocyclic aromatic organic compound with chemical formula C_9H_7N characterised by a double-ring structure containing benzene fused to pyridine at two adjacent carbon atoms. It is colourless hygroscopic liquid with strong odour [1,2]. Old samples when exposed to light turn to yellow and later to brown [3]. It is slightly soluble in cold water but readily in hot water and most organic solvents. Quinoline was first extracted from coal tar in 1834 by Friedlieb Ferdinand Runge [4] and named it "Leukol". It was also obtained in 1842 by Gerhardt through alkaline distillation and named it "Chinolein" or "Chinolin". Similarity between leukol and chinolin was established by Hoogewerff and Van Dorp in 1882. Dewar was the first to propose the correct structural formula for quinoline. Other names for quinoline include 1-azanaphthalene, 1-benzazine, benzazabenzene, benzopyridine, 1-benzine, chinoline and leucoline [1]. Quinoline yellow is used for dying textile such as silk, wool, nylon, and also for dying paper [5]. Compounds of quinoline family are broadly used to make drugs especially fungicides, biocides, alkaloids, dyes, rubber chemicals and flavouring agents. They are also used as catalyst, corrosion inhibitor and preservative [6]. Quinoline derivatives continued to attract attention for their applications in the field of anti-malarial [7-13], biological [14-17], anti-bacterial [18,19], anti-filarial [20] and anti-tuberculosis [21] activities. The derivatives of quinolines are also extensively used for receptor agonists [22-26], cardiovascular [27], and anti-neoplastic [28] activities.

Quinoline carboxaldehyde (QC) is a derivative of quinoline. In QC, aldehyde group is attached to quinoline. It has molecular formula of $C_{10}H_7NO$. Quinoline carboxaldehyde exhibits seven different positional isomers relative to carboxaldehyde

group namely; n-quinoline carboxaldehyde or quinoline-n-carboxaldehyde where n=2, 3, 4, 5, 6, 7, 8 representing the position of carboxaldehyde. This change in position of aldehyde group in quinoline ring leads to variation of structural parameters and charge distribution, and subsequently this affects chemical stability of the molecule. Quinoline carboxaldehyde is noted for its various applications. Quinoline-2-carboxaldehyde is an important component in the standard Henry reaction with variety of nitroalkanes [29]. Quinoline-3-carboxaldehyde and quinoline-4-carboxaldehyde are used in the sythesis of electron deficient complexes of biomedical important [30]. Quinoline-4-carboxaldehyde was also shown to form one-dimensional metal-organic coordination polymer [31]. Quinoline-6-carboxaldehyde is used in the synthesis of 1H-pyrrolo[2,3-f]quinoline-2-carboxamides [32]. Quinoline-8-carboxaldehyde also forms complexes with Palladium (II) and Platinum (II) [33]. For these reasons, understanding the spectral properties of quinoline and its derivatives is of great importance.

Both theoretical and experimental molecular properties of quinoline (electronic, Infrared, Raman, ^{1}H, ^{13}C, ^{14}N and ^{15}N NMR spectra) have been extensively studied [1,34,35]. Vibrational spectra of some quinoline carboxaldehyde isomers have been investigated recently [36-39]. However, thorough literature survey revealed that, there have been no reports on the electronic spectra of quinoline carboxaldehyde. Therefore, in the present study, the theoretical electronic absorption spectra in gas phase and water would be compared with the experimental spectra also in water for the seven isomers of quinoline carboxaldehyde. Conformational analysis, frontier molecular orbitals (FMOs), global chemical reactivity indices and molecular electrostatic potential (MESP) map would also be discussed. Quinoline carboxaldehyde would be abbreviated henceforth as QC.

CHAPTER 2

THEORETICAL BACKGROUND

2.1 ELECTRONIC ABSORPTION SPECTROSCOPY OF MOLECULES

The electronic spectra of molecules are found in the region of wavelength range of 100 to 700 nm of the electromagnetic spectrum. A region known as ultraviolet and visible (UV-vis) regions. The visible region, to which the human eye is sensitive, corresponds to the range of wavelengths between 400 and 700 nm. The ultra-violet region is subdivided into two spectral regions. The range between 200 and 400 nm is referred to as the near ultraviolet region. The region below 200 nm is called the far or vacuum ultra-violet region. Routine analysis is mainly done on the near-ultraviolet [40]. The visible region of the electromagnetic spectrum was discovered by Newton in 1764 and the ultraviolet region by J.W. Ritter in 1801 [41].

When a molecule absorbs radiation, its energy increases, this increase is equal to the energy of the photon as expressed by the relation

$$E = h\upsilon = \frac{hc}{\lambda} \tag{2.1}$$

where h is Planck's constant, υ and λ are the frequency and the wavelength of the radiation respectively and c is the velocity of light.

Absorption of UV-vis radiation by molecular absorbing species is a two-step process. Firstly the absorbing species is excited electronically upon absorbing photons

$$M + h\upsilon \rightarrow M* \tag{2.2}$$

Where M and M* are the species before and after excitation respectively and hυ is the photon energy. This process is very fast of the order of 10^{-8} to 10^{-9}s. The second step involves dissipation of the excess energy. Excited species can easily utilise their excess energy through various relaxation processes, most commonly through conversion of the excess energy into heat [42].

$$M* \rightarrow M + heat \tag{2.3}$$

Alternatively relaxation may occur through emitting the absorbed photons in a process known as luminescence. If the process took place fast then it is called fluorescence. In some cases the processes may occur slowly and it is termed as phosphorescence [43].

UV-vis absorption involves excitation of an electron from the ground state to higher excited state. The energy differences between electronic levels in most molecules vary from 125 to 650 kJ/mole [44]. The change in energy in the electronic energy level is accompanied by vibrational and rotational energy levels of the molecule. Quantum size of electronic transition is much greater than that of vibrational transition which in turn is much greater than that of rotational transition [45]. Many vibrational and rotational excitations to higher energy levels associated with higher excited states are possible. Therefore a molecule can be excited from the same electronic, vibrational and rotational energy levels to a single excited electron state but different vibrational and rotational energy levels [46]. Electronic transition has a coarse structure consisting of many vibrational transitions and fine structure consisting of many lines of rotational transitions. Fine structure can only be resolved with high resolution instrument. [47].

By Born-Oppenheimer approximation- the nuclei in a molecule are very heavier than the electrons, and therefore tend to move slowly- the total molecular wave function Ψ_{total}, can be approximated as the product of the wave functions of the three individual motions [47,48].

$$\Psi_{total} = \psi_e \psi_v \psi_r \tag{2.4}$$

The vibrational transitions that always accompany allowed electronic transition are called vibronic transitions. In electronic transition, there is no selection rule for the vibrational quantum number. However, vibronic transitions are observed not have the

same intensity. This is explained by the so called Franck-Condon Principle. It states that electronic transition in a molecule takes place so fast so that, in a vibronic transition the nuclei maintain the same position and velocity before and after the transition [45, 49, 52]. The intensities of vibronic transitions are governed by the value of

$$I \alpha \int \psi'_{Vib}(R)\psi''_{Vib}(R)dR \tag{2.5}$$

known as the vibrational overlap integral. Its square is known as the Franck-Condon factor [48, 49].

Figure 2.1(a) depicts a case where inter nuclear separation of upper and lower states are the same. According to Franck-Condon principle, transition occurs in a very short time, therefore transition is described by drawing vertical line drawn between the two potential curves. The most probable transition in Figure 2.1(a) is transition from A to B. Transition from A to C is unlikely to occur - though it maintains nuclei position – because the kinetic energy of the nuclear and inturn its velocity is increased in moving from B to C. In Figure 2.1(b), the internuclear separation of the two states is different. Transition from A to B is the most probable as nuclear remains stationary and maintains the same velocity. Transition from A to C is not possible because it involves change in inter nuclear separation. Likewise transition from A to D involves change in nuclear velocity and therefore it is not likely to occur [49].

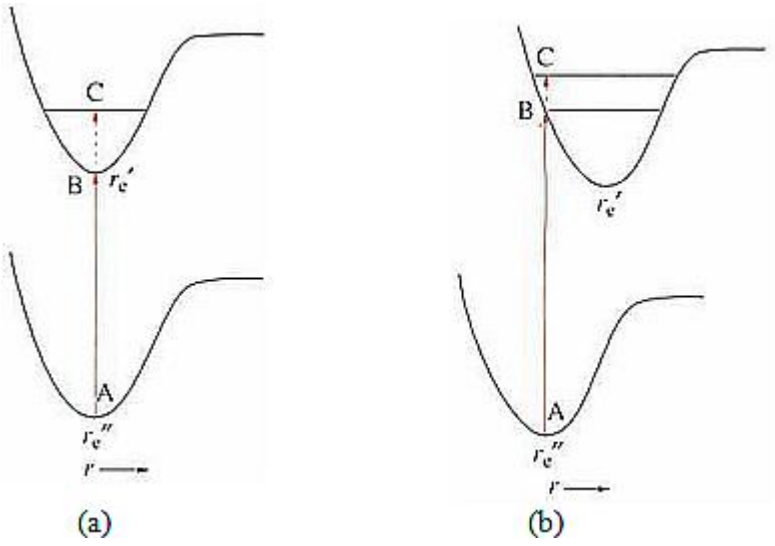

Figure 2.1 Franck-Condon principle for (a) $r'_e \approx r''_e$ and (b) $r'_e > r''_e$.

All organic compounds are capable of absorbing electromagnetic radiation because all contain valence electrons that can be excited to higher energy levels. [42]. Absorption occurs when a ground state electron in a bonding or non-bonding molecular orbital transition to anti-bonding orbital. The electrons that contribute to absorption by organic molecules are σ, π and n electrons. Molecular orbitals associated with single bonds in organic molecules are designated as σ orbitals and the corresponding electrons as σ electrons. σ orbital results from the overlap of two s orbitals, s orbital with p orbital or head-to-head overlap of two p orbitals. σ orbital has cylindrically symmetrical electron density around the internuclear axis. It corresponds to single bonds between atoms and to one of the bonds in double or triple bonds. π orbitals are formed by the parallel overlap of atomic p orbitals. Their charge distribution is characterised by a nodal plane along the axis of the bond and a miximum electron density in regions above and below the plane. π orbital has a cloud of electrons above and below the internuclear axis. n electrons are unshared electrons found in organic compounds with chromopore containing heteroatoms like oxygen, nitrogen, sulphur, chlorine, bromine, phosphorus etc. These electrons neither increases nor decreases the stability of a molecule [42, 46].

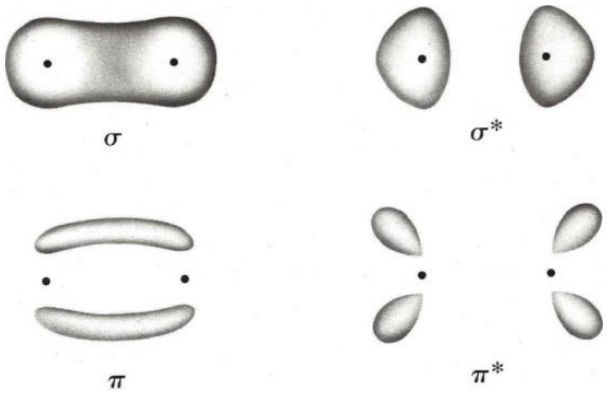

Figure 2.2 Bonding and anti-bonding molecular orbitals.

Four types of molecular electronic transitions that result from absorption of radiation whose magnitude falls in the UV-vis region are possible, viz., σ→σ*, n→σ*, π→π*, and n→π*.

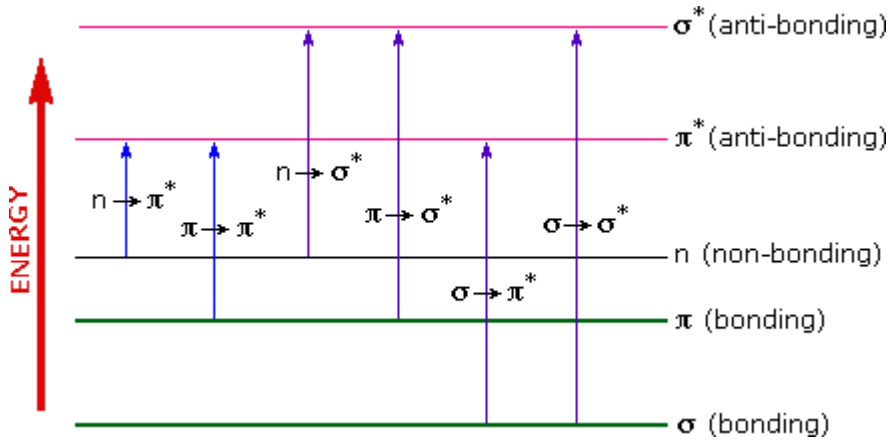

Figure 2.3 Energy levels of electronic transitions.

σ→σ* transition requires the greatest energy and is observed mainly in vacuum ultra-violet region (λ below 150 nm). Saturated compounds such as alkane with no non-bonding orbital can show this kind of transition. Because vacuum ultra-violet region is not accessible by spectrophotometers, absorption maxima due this transition are not observed under ordinary conditions and hence are not used in routine analysis. n→σ* transitions require less energy. Saturated hydrocarbons with non-bonding electron such as methyl chloride undergo this transition. π→π* and n→π* transitions are found in near-ultra violet region (200 to 700 nm). These are the most important transitions in chemical analysis. Both π→π* and n→π* transitions require the presence of an unsaturated functional group to provide π orbitals [40].

2.2 DENSTIY FUNCTIONAL THEORY

Density functional theory (DFT) is a quantum mechanical *ab initio* method used in Physics and Chemistry for the study of ground state electronic structures of quantum mechanical many-body systems, more precisely molecules and condensed matter phases [53]. The basic idea behind DFT is that the energy of an electronic system can be expressed as a function of electron probability density ρ(**r**) which in turn is a function depending only on three spatial coordinates. Hence the electronic energy is determined using functionals- functions of another functions- this gives rise to the name density functional theory [54-56].

DFT proves to be efficient and less demanding computationally even for fairly large systems when compared with Hartree-Fock method and its derivatives that use the

concept of electron wave function [57]. It produces results that generally agree with experiment. Another notable feature of DFT is that it accounted for exchange energy along with correlation energy. This is one of the reasons behind popularity of DFT. The concept of density functional was first introduced in 1927 through the works of L.H. Thomas and E. Fermi (working independently) to investigate the electronic structure of many-body system. The model was named after the two as Thomas-Fermi (TF) model [55,57,58]. However, TF model suffers some major drawbacks as the kinetic energy in it is poorly represented and it cannot describe molecular bonding [58]. In 1964 P. Hohenberg and W. Kohn give a formal proof of density functional asserting that the ground state electronic energy can be determine completely by electron density. But Hohenberg-Kohn theorem tells us nothing about the nature of the functional dependence of energy on the density it only proves its existence [57-59].

In KS-DFT, the Schrödinger equation for one-electron spin orbitals system has the form

$$\left[-\frac{1}{2}\nabla^2 - \sum_i \frac{Z_n}{|r-R_n|} + \int d^3\boldsymbol{r}'\rho(\boldsymbol{r}')\frac{1}{|r-r'|} + V_{XC}[\rho]\right]\Psi_i(\mathbf{r}) = \varepsilon_i\Psi_i(\mathbf{r}) \qquad (2.6)$$

The first term in the left side of Eq. (2.6) represents the kinetic energy of the electrons; the second term represents the electron–nucleus attraction; the third term represents the Coulomb interaction between the total charge distributions. The last term is the exchange–correlation energy of the system. $E_{XC}[\rho]$ takes into account all non-classical electron-electron interactions. Among these terms, $E_{XC}[\rho]$ is the one we do not know exactly but according to HK-theorem E and $E_{XC}[\rho]$ are functional of ρ(**r**), we don't know the exact analytical form of $E_{XC}[\rho]$ and so are forced to make approximate expression for it. The exact ground-state electron density is given by

$$\rho(\boldsymbol{r}) = \sum_{i=1}^{n}|\psi_i(\boldsymbol{r})|^2 \qquad (2.7)$$

where the sum is over all the occupied Kohn–Sham (KS) orbitals. For many- electron system the total energy is given by

$$E = \sum_{i=1}^{N}\varepsilon_i - \frac{1}{2}\int d^3\boldsymbol{r}d^3\boldsymbol{r}'\rho(\boldsymbol{r})\frac{1}{|r-r'|}\rho(\boldsymbol{r}') + E_{XC}[\rho] - \int d^3\boldsymbol{r}V_{XC}[\rho]\,\rho(\boldsymbol{r}) \qquad (2.8)$$

ε_i is the KS orbital energies and V_{XC} is the functional derivative of E_{XC} given by [56]

$$V_{XC}[\rho] = \frac{\delta E_{XC}[\rho]}{\delta \rho} \quad (2.9)$$

Several approaches have been deviced for obtaining approximate forms for the exchange—correlation energy functional. The main source of error in DFT usually arises from the approximate nature of $E_{XC}[\rho]$. A primitive approach is the local density approximation, LDA. The density is assumed to be uniform throughout the system as in uniform electron gas. But this is not always true though it has yielded some accurate results especially in the prediction of structural properties [55]. To improve LDA approach, generalized gradient approximation (GGA) was developed. In GGA exchange and correlation terms are made to depend not only on the electron density but also on the gradient of the density. One of the famous GGA was developed by Becke. Other GGA functionals are PW86 (Perdew –Wang 1986), PW91 (Perdew-Wang 1991), PBE (Perdew, Burke and Ernzerhof), etc [60]. Further advancement beyond GGA functionals continued to appear. Based on that, hybrid-functional that utilises Hartree-Fock corrections co-jointly with density functional correction and exchange was developed. One of the best functional in quantum chemistry is B3LYP. This is a combination of the Lee-Yang-Parr (LYP) GGA for correlation with Becke's three-parameter hybrid functional B3 for exchange [55].

2.3 COMPUTATIONAL DETAILS

All computations were performed using GAUSSIAN03 programme [61]. The initial structure of QC molecules were modeled with the GaussView programme [62] and was later optimised in gas phase using the Becke's three parameter hybrid functional in conjunction with Lee-Yang-Parr correlation functional (B3LYP); hybrid DFT functional with the 6-311G++(d,p) basis set. This basis set adds polarisation functions of three p-type polarisation functions and one s-type diffuse function to the hydrogen atom as well as five d-type functions and one p-type function on atoms other than hydrogen atoms [38]. The inclusion of extra polarisation functions does not affect the excitation energies [63]. These optimised geometries were then subjected to 40 state TD-B3LYP [64] in gas phase and water solvent to obtain vertical electronic absorption spectra wavelengths with their corresponding oscillator strengths.

The bulk solvent effects were treated using the standard polarisable continuum model (PCM). In PCM one devides the problem into a solute part (in our case QC) lying

inside a cavity, and a solvent part (here water) as a structureless material, characterised by its dielectric constant and other macroscopic properties such as density, molecular volume etc. PCM can only give valid approximation as far as there is no specific interaction such as hydrogen bonds between the solute and the solvent molecules [63,65-69]. For excited states, there are two kind of PCM model: equilibrium and non-equilibruim solutions. For the study of UV-vis spectra, we have selected the non-equilibruim PCM solutions because only the solvent electronic distribution can instantenously adapt to the new (excited) electronic structure of the solute, while molecular motions of the solvent are frozen during the process [65].

The MESP and FMOs were plotted using GaussView [62] after the TD-DFT calculations.

CHAPTER 3

EXPERIMENTAL STUDIES

3.1 INSTRUMENTATION

Spectrophotometer is the instrument used to measure UV-vis absorption spectrum. Spectrophotomteres are classified as single and double-beam instruments according to the type of wavelength selector and detector. Both single and double-beam spectrophotometers are used in UV-vis absorption spectroscopy. In a single-beam instrument, one beam of radiation is used and passes through a single cell. It is primarily used for studies performed at a single wavelength. Double-beam instrument divides the incident radiation into two beams and passed them through two separate cells. One of the cells is filled with pure solvent and the second cell is filled with the sample solution. Double-beam instruments can be used at a fixed wavelength or to scan through a wavelength region. Double-beam instruments have the advantage of eliminating variations in intensity of the radiative source or variations in electronic response of the detectors [46]. A typical spectrophotometer comprises of the following components: Radiation source, Monochromator, Sample container, Detector, Readout devices as shown in Figure 3.1.

Sources; for the purpose of molecular spectroscopy, a radiation source which is continuum, durable, stable and constant over a considerable range of wavelengths is required. The common sources of radiation used are deuterium lamp, tungsten and xenon arc lamp. Tungsten filament lamp is the most common source of visible and near infra-red radiation. Its radiation when heated equalise to that of blackbody radiation [42,46]. It provides radiation from about 350 to 3500 nm [46]. In the UV region, Hydrogen and Deuterium lamps are used as radiation source through electrical

excitation at low pressure [42]. Hydrogen and Deuterium provide continuous radiation from about 180 to 350 nm [46]. Xenon arc lamp produces radiation by the passage of current through an atmosphere of xenon. The spectrum is continuum over the range of 200 to 1000 nm [42].

Monochromator; separates or disperses the radiation so that the frequencies corresponding to particular energy transitions within the sample can be examined individually. Polychromatic radiation entering the monochromator is directed on to a narrow entrance slit and from there to the prism or grating. By rotating the prism or grating, radiation of different frequencies and consisting of sharp images of the entrance slit can be made to pass successively through a fixed exit slit and on to the detector. If the output from the detector is fed to the chart recorder, a continuous trace of the spectrum is obtained. Alternatively, a photographic film or plate or a series of exit slits and detectors positioned along the focal plane of the monochromator enables radiation of many frequencies to be detected simultaneously without rotating the prism or grating [46].

Sample containers; in most cases, the sample under investigation is dissolved in solvent forming solution of the absorbing substance. The solution is held in place in the path of radiation in a cell or cuvette. The cell or cuvette that hold the solution of sample should be made of material that is transparent to radiation in the spectral region of study. In the visible region glass can be used. However, glass absorbs radiation in ultra-violet region, and the cell that is used in the ultra-violet region is usually made of quartz or fused silica. Quartz and silica are also transparent in the visible region. Cells are usually made in rectangular form with parallel transparent windows through which the radiation passes. For most routine analysis, a cell with a 1 cm path length is convinient [42,46].

Detectors; detector converts the intensity of the light reaching it to an electric signal [70]. Photoelectric transducers are used as detection devices in most modern instruments. Photo electric transducer converts photons into electrical signal. Several forms of transducers include barrier layer cells, photomultiplier tubes and semiconductor detectors. Most modern instruments employ photoelectric transducers. Photoelectric transducers have a surface that can absorb radiant energy. The absorbed energy either causes the emission of electrons, resulting in a photocurrent or moves

electrons into the conduction band of a solid semiconductor, resulting in an increase in conductivity [71].

Readout devices; A large variety of readout devices are available in spectrophotometers. Those that are encountered most often include analogue metres, digital metres, printers or video diplays. Scanning instruments use recorders, computer-controlled recorders, xy plotters, video displays or combination of computer-controlled recorders or plotters and printers [46].

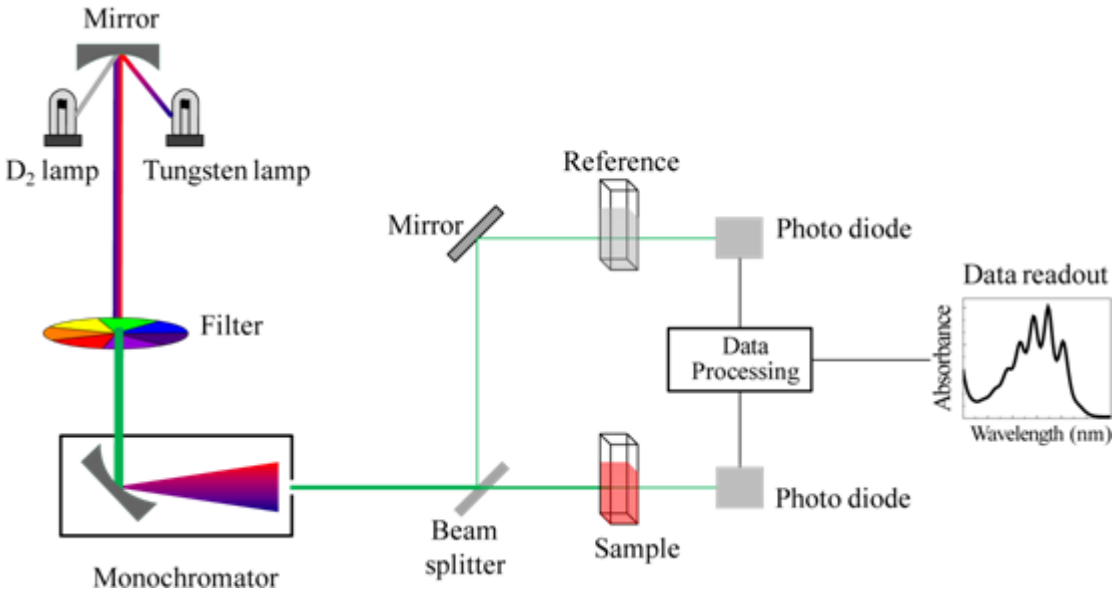

Figure 3.1 Schematic diagram of double-beam spectrophotometer.

3.2 LAMBERT- BEER LAW

In routine analysis, molecular absorption of ultraviolet or visible radiation is measured by passing monochromatic radiation through the sample. The radiation absorbed by the sample is determined by comparing the intensity of the transmitted radiation through the solvent with no absorbing sample to the transmitted radiation in the present of the sample [40]. When light passes through cell containing the sample, some of the photons in the incident radiation are absorbed by the sample, some reflected by the cell walls and some scattered by suspended particles in the cell. Therefore the intensity of the incident radiation is decreased [46] as shown in Figure 3.2.

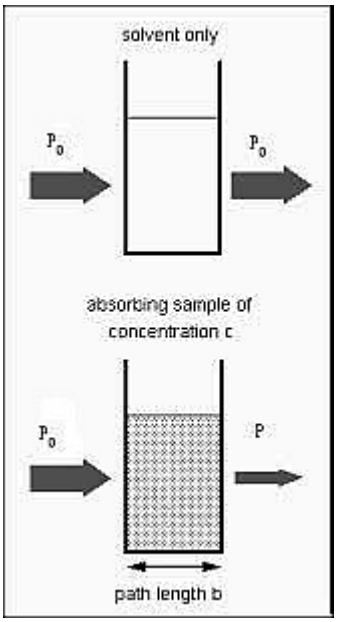

Figure 3.2 Absorption process.

If the incident radiation is designated as P_0 and the transmitted one after passing through the sample cell as P then transmittance T can be written as

$$T = \frac{P}{P_0} \tag{3.1}$$

A peculiar law which relates the absorbance A, radiation path length b and concentration of the absorbing specie C is known as Lambert-Beer- Bouguer, Lambert - Beer law or simply Beer's law and is given as

$$A = \varepsilon bC \tag{3.2}$$

ε is called molar extinction coefficient and is constant for a given sample and depends on wavelength. Its unit depends on those of b and C. if C is measured in molarity and b in centimetre then its unit is given by $Lmol^{-1}cm^{-1}$. If C and b are measured in other units then ε is replaced by *a* and is called specific absorptivity [40,46,71]. Extinction coefficient ranging from zero to 10^4 $Lmol^{-1}cm^{-1}$ is usually observed in UV-vis spectromerty [42,44].

3.3 EXPERMENTAL DETAILS

The entire samples were obtained from Alfa Aeser USA each with a stated purity of 97+% except for Q7C which is obtained from Tokyo Chemical Industry Co. and the samples were used as received without further purification. The UV-vis absorption spectra of the compounds were measured in water as solvent. A small amount of the samples were dissolved in water and stirred vigorously using magnetic stirrer leading to colourless solution of the samples. Measurements were completed using Thermo Scientific Evolution 300 spectrophotometer at room temperature. Xenon arc lamp was used as radiation source and the scan region was set as 190-1100 nm. However the samples show absorption bands only in the region of 200-400 nm. Quartz cells with a path length of 1cm and a $3cm^3$ volume were used for all measurements.

CHAPTER 4

RESULTS AND DISCUSSIONS

4.1 MOLECULAR GEOMETRY

QC has a planar structure; therefore it belongs to C_S points group. Figure 4.1 shows the optimised structures of the two rotamers of QC molecules. Rotamer 1 (Rot1) and Rotamer 2 (Rot2) represent the spatial orientation of CHO. When C=O is farther away than N atom of quinoline we call the conformation as rotamer 1 (Rot1). When it is closer to N atom, we call it as rotamer 2 (Rot2) [38]. In order to find the most stable rotamer, energy calculations were carried out for QC molecules at B3LYP/6-311G++(d,p) level for the two different rotamers. The Rot1's are found to have less energy compared to Rot2's and hence are more stable. The stability of Rot1 could possibly be due acceptor-donor pair formed by nitrogen atom of the pyridine ring and hydrogen atom of carboxaldehyde moiety while the destabilty of Rot2 could be due to repulsive interaction between nitrogen atom of the pyridine ring and oxygen atom of carboxaldehyde moiety.

All *ab initio* results reported herein are of the more stable rotamers; Rot1 [72,73]. The optimised structural parameters (bond length and bond angle) of the stable rotomers (Rot1) are reported in Table 4.1 to 4.7 in accordance with the atomic numbering shown in Figure 4.1. There is no experimental data on the structure of QC which could be compared with the calculated result available in literature to the best of our knowledge.

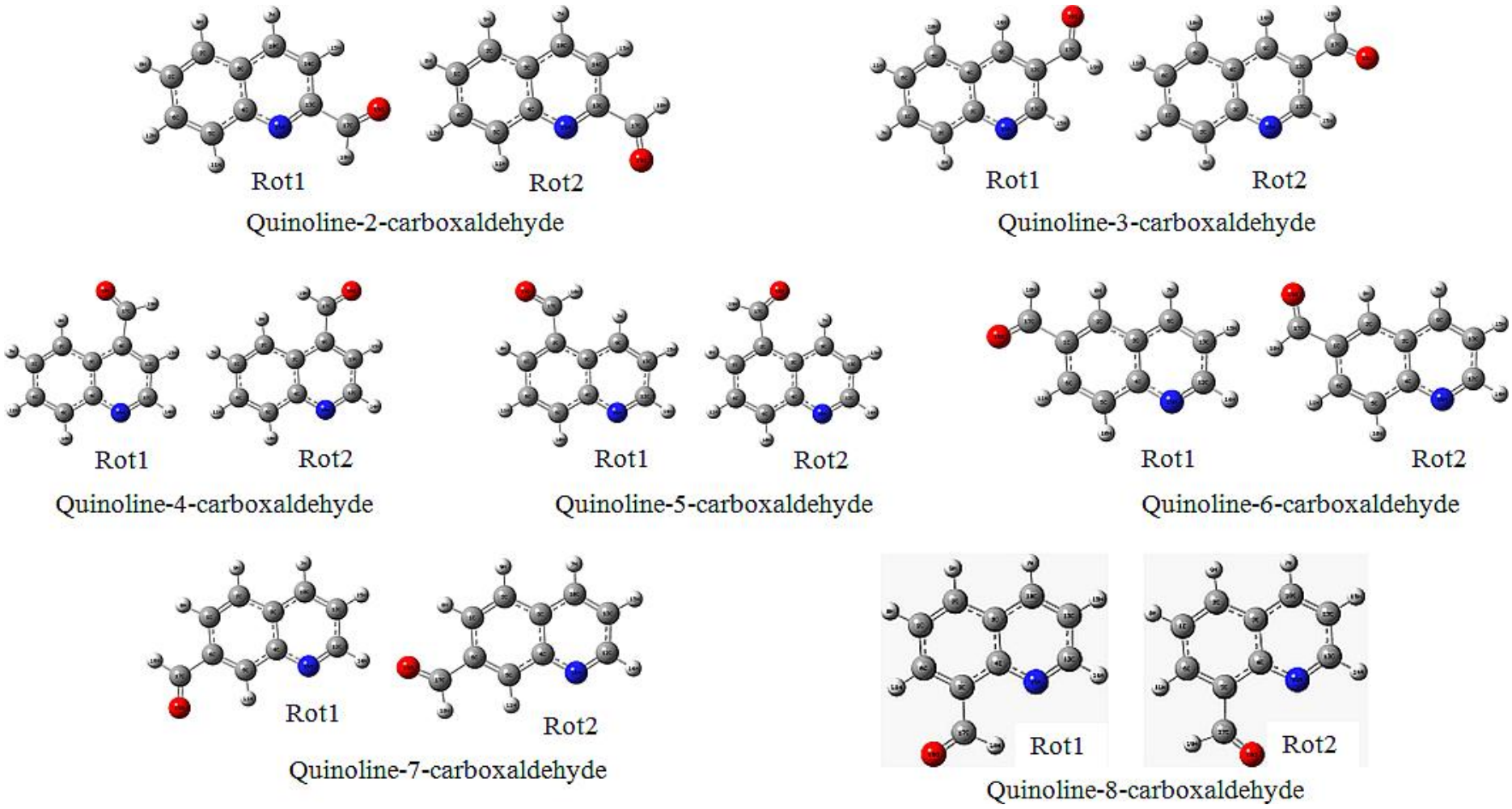

Figure 4.1 Optimised geometry of Rot1 and Rot2 conformers of QC derivatives.

Table 4.1 Optimised geometrical parameters of Q2C at the B3LYP/6-311++G(d,p) level.

Bond length (Å)		Bond angle (^{o})	
C1—C 2	1.375	C2—C1—C6	120.5
C1—C6	1.416	C2—C1—H8	120.0
C1—H8	1.084	C6—C1—H8	119.5
C2—C3	1.417	C1—C2—C3	120.4
C2—H9	1.085	C1—C2—H9	120.6
C3—C4	1.432	C3—C2—H9	119.0
C3—C10	1.418	C2—C3—C4	119. 1
C4—C5	1.419	C2—C3—C10	123.3
C4—N16	1.359	C4—C3—C10	117.6
C5—C6	1.374	C3—C4—C5	119. 2
C5—H11	1.083	C3—C4—N16	122. 1
C6—H12	1.084	C5—C4—N16	118.7
C10—H7	1.085	C4—C5—C6	120.3
C10—C14	1.370	C4—C5—H11	117.8
C13—C14	1.419	C6—C5—H11	121.9
C13—N16	1.320	C1—C6—C5	120.5
C13—C17	1.493	C1—C6—H12	119.4
C14—H15	1.083	C5—C6—H12	120.0
C17—H18	1.107	C3—C10—H7	119.4
C17—O19	1.210	C3—C10—C14	119.6
		H7—C10—C14	121.0
		C14—C13—N16	124.1
		C14—C13—C17	120.6
		N16—C13—C17	115.3
		C10—C14—C13	118.4
		C10—C14—H15	122.6
		C13—C14—H15	118.9
		C4—N16—C13	118.2
		C13—C17—H18	113.6
		C13—C17—O19	124.1
		H18—C17—O19	122.4

Table 4.2 Optimised geometrical parameters for Q3C at the B3LYP/6-311++G(d,p) level.

Bond length (Å)		Bond angle (^{o})	
C1—C2	1.375	C2—C1—C6	120.8
C1—C6	1.417	C2—C1—H7	119.8
C1—H7	1.084	C6—C1—H7	119.3
C2—C3	1.417	C1—C2—C3	120.3
C2—H8	1.083	C1—C2—H8	121.8
C3—C4	1.434	C3—C2—H8	117.9
C3—N16	1.365	C2—C3—C4	118.9
C4—C5	1.421	C2—C3—N16	118.6
C4—C9	1.409	C4—C3—N16	122.5
C5—C6	1.373	C3—C4—C5	119.3
C5—H10	1.085	C3—C4—C9	117.6
C6—H11	1.084	C5—C4—C9	123.1
C9—C12	1.381	C4—C5—C6	120.3
C9—H14	1.085	C4—C5—H10	118.9
C12—C13	1.421	C6—C5—H10	120.8
C12—C17	1.479	C1—C6—C5	120.3
C13—H15	1.089	C1—C6—H11	119.6
C13—N16	1.312	C5—C6—H11	120.2
C17—O18	1.211	C4—C9—C12	119.4
C17—H19	1.110	C4—C9—H14	121.0
		C12—C9—H14	119.7
		C9—C12—C13	118.4
		C9—C12—C17	121.6
		C13—C12—C17	120.0
		C12—C13—H15	119.1
		C12—C13—N16	124.4
		H15—C13—N16	116.5
		C3—N16—C13	117.8
		C12—C17—O18	124.7
		C12—C17—H19	114.8
		O18—C17—H19	120.5

Table 4.3 Optimised geometrical parameters of Q4C at the B3LYP/6-311++G(d,p) level.

Bond length (Å)		Bond angle (^{o})	
C1—C2	1.377	C2—C1—C6	121.0
C1—C6	1.413	C2—C1—H7	119.5
C1—H7	1.084	C6—C1—H7	119.5
C2—C3	1.419	C1—C2—C3	120.3
C2—H8	1.080	C1—C2—H8	120.7
C3—C4	1.435	C3—C2—H8	119.0
C3—C9	1.432	C2—C3—C4	118.6
C4—C5	1.418	C2—C3—C9	124.7
C4—N16	1.364	C4—C3—C9	116.7
C5—C6	1.373	C3—C4—C5	119.5
C5—H10	1.083	C3—C4—N16	123.1
C6—H11	1.084	C5—C4—N16	117.4
H8—O18	2.257	C4—C5—C6	120.4
C9—C13	1.381	C4—C5—H10	117.5
C9—C17	1.486	C6—C5—H10	122.0
C12—C13	1.412	C1—C6—C5	120.2
C12—H14	1.087	C1—C6—H11	119.7
C12—N16	1.313	C5—C6—H11	120.1
C13—H15	1.085	C3—C9—C13	118.6
C17—O18	1.210	C3—C9—C17	125.1
C17—H19	1.110	C13—C9—C17	116.3
		C13—C12—H14	119.9
		C13—C12—N16	123.3
		H14—C12—N16	116.7
		C9—C13—C12	120.0
		C9—C13—H15	120.3
		C12—C13—H15	119.7
		C4—N16—C12	118.4
		C9—C17—O18	126.9
		C9—C17—H19	112.9
		O18—C17—H19	120.2

Table 4.4 Optimised geometrical parameters of Q5C at the B3LYP/6-311++G(d,p) level.

Bond length (Å)		Bond angle (^{o})	
C1—C2	1.401	C2—C1—C6	120. 0
C1—C6	1.401	C2—C1—H8	120.0
C1—H8	1.070	C6—C1—H8	120.0
C2—C3	1.401	C1—C2—C3	119.9
C2—C17	1.540	C1—C2—C17	120.0
C3—C4	1.402	C3—C2—C17	120.0
C3—C9	1.395	C2—C3—C4	120.3
C4—C5	1.402	C2—C3—C9	120.3
C4—N16	1.344	C4—C3—C9	119.4
C5—C6	1.402	C3—C4—C5	119.7
C5—H10	1.070	C3—C4—N16	120.6
C6—H11	1.070	C5—C4—N16	119.7
H7—C9	1.070	C4—C5—C6	120.1
C9—C13	1.395	C4—C5—H10	120.0
C12—C13	1.402	C6—C5—H10	120.0
C12—H14	1.070	C1—C6—C5	120.0
C12—N16	1.344	C1—C6—H11	120.0
C13—H15	1.070	C5—C6—H11	120.0
C17—H18	1.366	C3—C9—H7	120.6
C17—O19	1.434	C3—C9—C13	118.8
		H7—C9—C13	120.6
		C13—C12—H14	119.7
		C13—C12—N16	120.6
		H14—C12—N16	119.7
		C9—C13—C12	119.4
		C9—C13—H15	120.3
		C12—C13—H15	120.3
		C4—N16—C12	121.2
		C2—C17—H18	110.0
		C2—C17—O19	111.9
		H18—C17—O19	136.7

Table 4.5 Optimised geometrical parameters of Q6C at the B3LYP/6-311++G(d,p) level.

Bond length (Å)		Bond angle (^{o})	
C1—C2	1.380	C2—C1—C6	120.2
C1—C6	1.422	C2—C1—C17	119.3
C1—C17	1.480	C6—C1—C17	120.5
C2—C3	1.415	C1—C2—C3	120.7
C2—H8	1.087	C1—C2—H8	120.0
C3—C4	1.431	C3—C2—H8	119.3
C3—H9	1.417	C2—C3—C4	119.0
C4—C5	1.423	C2—C3—H9	123.4
C4—N16	1.361	C4—C3—H9	117.7
C5—C6	1.369	C3—C4—C5	119.1
C5—H10	1.083	C3—C4—N16	122.3
C6—H11	1.083	C5—C4—N16	118.6
H7—C9	1.085	C4—C5—C6	120.6
C9—C13	1.372	C4—C5—H10	117.6
C12—C13	1.416	C6—C5—H10	121.8
C12—H14	1.087	C1—C6—C5	120.4
C12—N16	1.316	C1—C6—H11	118.2
C13—H15	1.083	C5—C6—H11	121.4
C17—H18	1.111	C3—C9—H7	119.6
C17—O19	1.211	C3—C9—C13	119.2
		H7—C9—C13	121.2
		C13—C12—H14	119.5
		C13—C12—N16	124.3
		H14—C12—N16	116.2
		C9—C13—C12	118.7
		C9—C13—H15	121.5
		C12—C13—H15	119.8
		C4—N16—C12	117.9
		C1—C17—H18	114.6
		C1—C17—O19	124.8
		H18—C17—O19	120.6

Table 4.6 Optimised geometrical parameters of Q7C at the B3LYP/6-311++G(d,p) level.

Bond length (Å)		Bond angle (°)	
C1—C2	1.372	C2—C1—C6	120.6
C1—C6	1.419	C2—C1—H8	120.3
C1—H8	1.085	C6—C1—H8	119.2
C2—C3	1.419	C1—C2—C3	120.3
C2—H9	1.085	C1—C2—H9	120.6
C3—C4	1.432	C3—C2—H9	119.1
C3—C10	1.418	C2—C3—C4	119.4
C4—C5	1.413	C2—C3—C10	123.2
C4—N16	1.366	C4—C3—C10	117.4
C5—C6	1.382	C3—C4—C5	119.1
C5—C11	1.083	C3—C4—N16	122.5
C6—C17	1.484	C5—C4—N16	118.5
H7—C10	1.085	C4—C5—C6	120.4
C10—C13	1.371	C4—C5—C11	119.1
C12—C13	1.419	C6—C5—C11	120.5
C12—H14	1.087	C1—C6—C5	120.3
C12—N16	1.313	C1—C6—C17	119.1
C13—H15	1.084	C5—C6—C17	120.7
C17—H18	1.111	C3—C10—H7	119.6
C17—O19	1.210	C3—C10—C13	119.2
		H7—C10—C13	121.2
		C13—C12—H14	119.5
		C13—C12—N16	124.1
		H14—C12—N16	116.4
		C10—C13—C12	118.9
		C10—C13—H15	121.4
		C12—C13—H15	119.7
		C4—N16—C12	117.9
		C6—C17—H18	114.5
		C6—C17—O19	125.1
		H18—C17—O19	120.5

Table 4.7 Optimised geometrical parameters of Q8C at the B3LYP/6-311++G(d,p) level.

Bond length (Å)		Bond angle (^{o})	
C1—C2	1.373	C2—C1—C6	119.6
C1—C6	1.409	C2—C1—H8	120.6
C1—H8	1.084	C6—C1—H8	119.9
C2—C3	1.419	C1—C2—C3	120.6
C2—H9	1.085	C1—C2—H9	120.6
C3—C4	1.433	C3—C2—H9	118.8
C3—C10	1.416	C2—C3—C4	120.1
C4—C5	1.437	C2—C3—C10	122.0
C4—N16	1.357	C4—C3—C10	117.8
C5—C6	1.384	C3—C4—C5	118.3
C5—C17	1.491	C3—C4—N16	121.7
C6—H11	1.086	C5—C4—N16	120.0
H7—C10	1.085	C4—C5—C6	119.1
C10—C13	1.371	C4—C5—C17	125.4
C12—C13	1.414	C6—C5—C17	115.5
C12—H14	1.088	C1—C6—C5	122.3
C12—N16	1.315	C1—C6—H11	119.2
C13—H15	1.084	C5—C6—H11	118.5
C17—O18	1.205	C3—C10—H7	119.4
C17—H19	1.114	C3—C10—C13	119.4
		H7—C10—C13	121.2
		C13—C12—H14	119.6
		C13—C12—N16	124.3
		H14—C12—N16	116.1
		C10—C13—C12	118.3
		C10—C13—H15	121.6
		C12—C13—H15	120.1
		C4—N16—C12	118.5
		C5—C17—O18	128.5
		C5—C17—H19	111.5
		O18—C17—H19	120.0

4.2 UV-VIS SPECTRAL ANALYSIS

TD-DFT/B3LYP/6-311++G(d,p) is used to simulate the UV-vis absorption spectra of the QC molecules. Figures 4.2 to 4.9 depict the experimental and calculated UV-vis absorption spectra of the title molecules. The inclusion of solvent effect of water leads to slight bathochromic shift (red shift) in the absorption spectra. Tables 4.8 to 4.14 show the calculated excitation energies (*E*), oscillator strengths (*f*) and wavelengths (λ) along with the experimental wavelengths for each molecule. Oscillator strength *f* is a dimensionless quantity that describes the strength of an electronic transition. It is the ratio of the strength of the transition to that of an electric dipole transition between two states of an electron oscillating in three dimensions in a simple harmonic way, and its maximum value is 1. Transitions with extremely low *f* values of order of 10^{-4} are forbidden [47,54,74].

The simulated spectra show good agreement with experimental spectra. However, simulated spectra of Q2C, Q3C, Q4C, Q6C and Q7C show some additional bands (224 and 342 nm in water and 218 and 322 nm in gas for Q2C, 335 nm in water and 326 nm in gas for Q3C, 356 nm in water and 352 nm in gas for Q4C, 315 nm in water and 309 nm in gas for Q6C, 326 nm in water and 315 nm in gas for Q7C) that were not observed in the experimental spectra. These additional bands have very low *f* value and are considered forbidden. Therefore, the bands can only be predicted theoretically but experimentally unfeasible. The experimental bands appear to be broader than the simulated bands. This is due to π-π stacking since the tittle molecules contain many π orbitals. It can be observed generally that the oscillator strength increases when moving from gas to solvent environment.

The aborption bands of Q2C, Q4C and Q5C in which the carboxaldehyde group is located at ortho position are observed to be shifted to the blue region. Q3C, Q6C and Q7C in which the carboxaldehyde is located at para positions have longer wavelength and hence are shifted to the red region. The λ_{max} shifts when changing the position of carboxaldehyde group is in general small. The nature of substituents (electron releasing or electron withdrawing) may affect the electronic structure of the ring system.

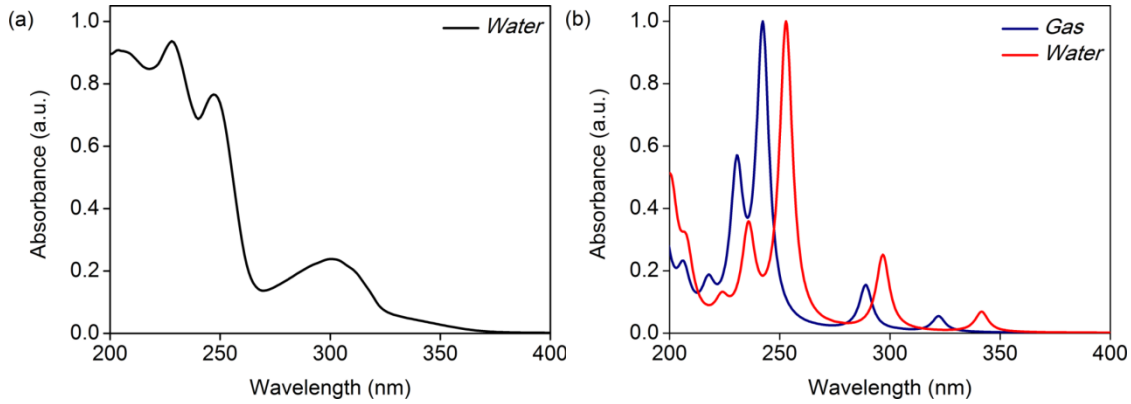

Figure 4.2 (a) Experimental and (b) Theoretical spectra of Q2C.

Table 4.8 Experimental and theoretical values for Q2C.

Experimental	Calculated			
Water	Water			
λ (nm)	λ (nm)	E (eV)	f	MO contribution
205	207	5.99	0.14	HOMO-1→LUMO+2,HOMO→LUMO+2
-	224	5.55	0.05	HOMO-4→LUMO,HOMO→LUMO+4
228	236	5.25	0.21	HOMO-1→LUMO+1,HOMO→LUMO+2
247	253	4.90	0.70	HOMO→LUMO+1,HOMO-1→LUMO
301	297	4.17	0.17	HOMO-1→LUMO
-	342	3.63	0.05	HOMO→LUMO,HOMO-1→LUMO+1
	Gas			
	206	6.02	0.08	
	218	5.69	0.06	
	231	5.37	0.28	
	242	5.12	0.56	
	289	4.29	0.09	
	322	3.85	0.03	

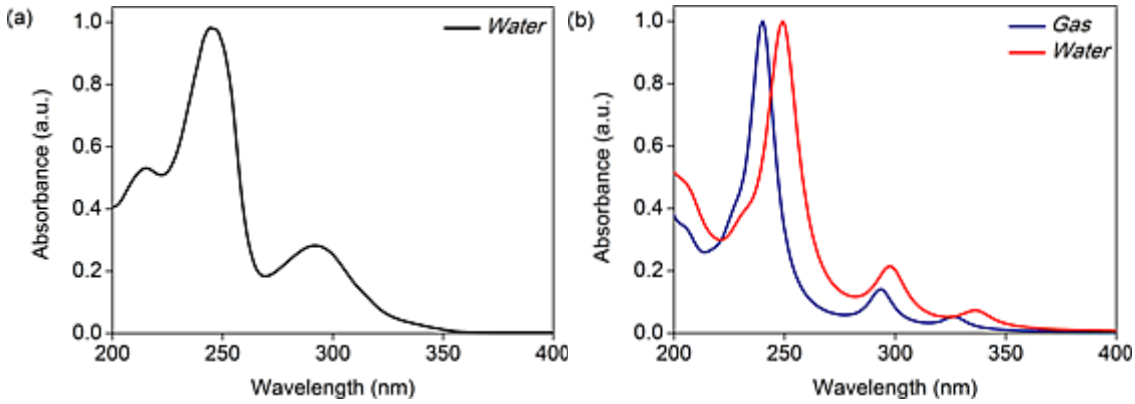

Figure 4.3 (a) Experimental and (b) Theoretical spectra for Q3C.

Table 4.9 Experimental and theoretical values for Q3C.

Experimental	Calculated			
Water	Water			
λ (nm)	λ (nm)	E (eV)	f	MO contribution
215	207	5.99	0.17	HOMO→LUMO+2,HOMO→LUMO+1
245	249	4.98	0.88	HOMO→LUMO,HOMO-1→LUMO+2
293	297	4.17	0.16	HOMO-1→LUMOHOMO→LUMO+1
-	335	3.70	0.05	HOMO→LUMO,HOMO-1→LUMO
	Gas			
	204	6.08	0.11	
	240	5.17	0.76	
	293	4.23	0.09	
	326	3.80	0.03	

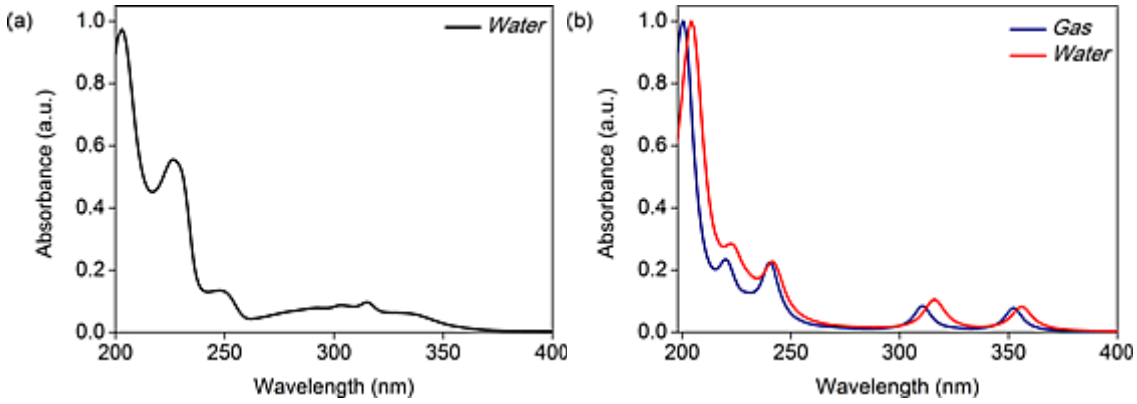

Figure 4.4 (a) Experimental and (b) Theoretical spectra for Q4C.

Table 4.10 Experimental and theoretical values for Q4C.

Experimental	Calculated			
Water	Water			
λ (nm)	λ (nm)	E (eV)	f	MO contribution
203	204	6.08	0.75	HOMO-1→LUMO+1,HOMO→LUMO+2
227	222	5.58	0.17	HOMO-4→LUMO,HOMO-1→LUMO+1
250	242	5.12	0.20	HOMO→LUMO+1,HOMO-1→LUMO+2
315	316	3.92	0.11	HOMO-1→LUMO
	356	3.48	0.09	HOMO→LUMO,HOMO-4→LUMO
	Gas			
	200	6.20	0.42	
	220	5.64	0.13	
	239	5.19	0.17	
	310	4.00	0.07	
	352	3.52	0.07	

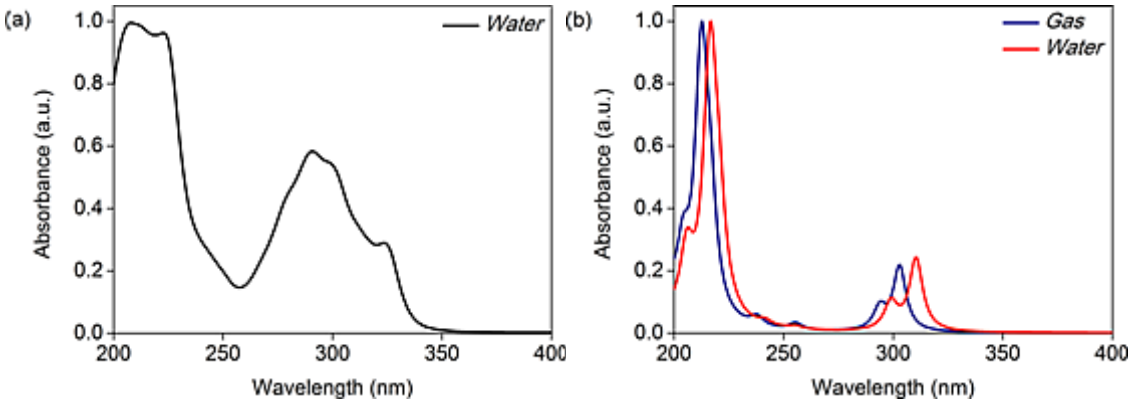

Figure 4.5 (a) Experimental and (b) Theoretical spectra for Q5C.

Table 4.11 Experimental and theoretical values for Q5C.

Experimental	Calculated			
Water	Water			
λ (nm)	λ (nm)	E (eV)	f	MO contribution
208	206	6.02	0.20	HOMO-2→LUMO+2,HOMO-5→LUMO
223	217	5.71	0.81	HOMO→LUMO+2,HOMO-2→LUMO+1
291	299	4.15	0.08	HOMO-2→LUMO,HOMO→LUMO+2
324	310	4.00	0.22	HOMO→LUMO,HOMO-2→LUMO
	Gas			
	204	6.08	0.14	
	213	5.82	0.61	
	294	4.21	0.05	
	303	4.09	0.15	

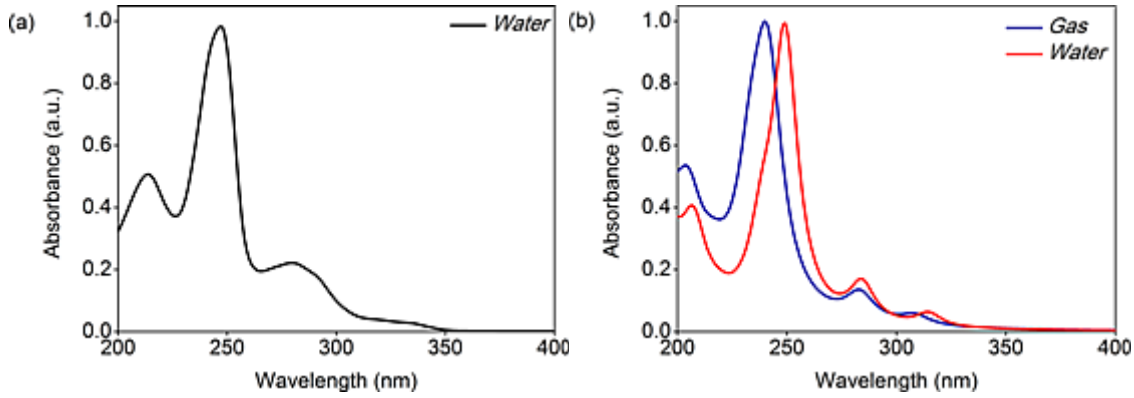

Figure 4.6 (a) Experimental and (b) Theoretical spectra for Q6C.

Table 4.12 Experimental and theoretical values for Q6C.

Experimental	Calculated			
Water	Water			
λ (nm)	λ (nm)	E (ev)	f	MO contribution
213	207	5.99	0.27	HOMO→LUMO+2,HOMO-4→LUMO+1
247	249	4.98	0.91	HOMO→LUMO+2,HOMO-1→LUMO+1
280	284	4.37	0.12	HOMO-1→LUMO,HOMO→LUMO+1
-	315		0.04	HOMO→LUMO
	Gas			
	204	6.08	0.25	
	240	5.17	0.62	
	283	4.38	0.07	
	309		0.02	

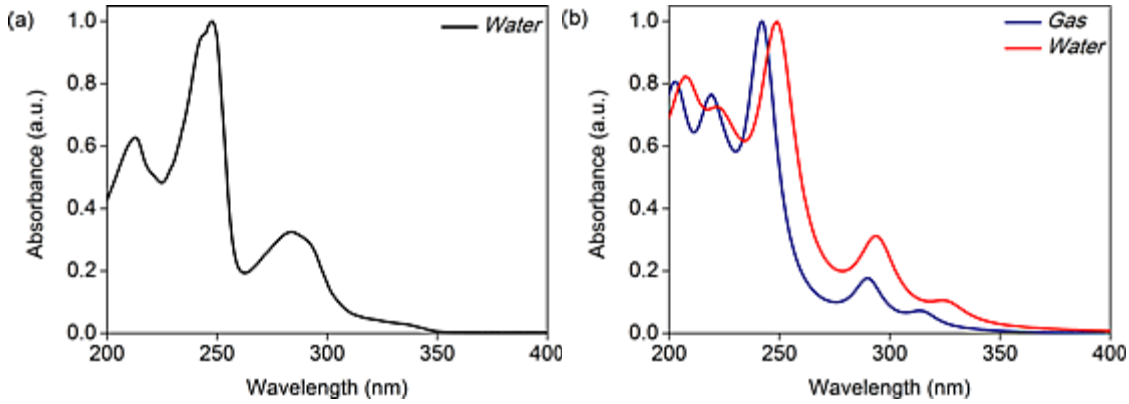

Figure 4.7 (a) Experimental and (b) Theoretical spectra for Q7C.

Table 4.13 Experimental and theoretical values for Q7C.

Experimental	Calculated			
Water	Water			
λ (nm)	λ (nm)	E (eV)	f	MO contribution
213	207	5.99	0.40	HOMO→LUMO+2,HOMO-4→LUMO
-	222	5.58	0.25	HOMO-4→LUMO
248	249	4.98	0.67	HOMO→LUMO+1
285	294	3.80	0.19	HOMO-1→LUMO,HOMO→LUMO+1
-	326	3.80	0.04	HOMO→LUMO
	Gas			
	203	6.11	0.32	
	220	5.64	0.29	
	242	5.12	0.57	
	290	4.19	0.09	
	315	3.94	0.03	

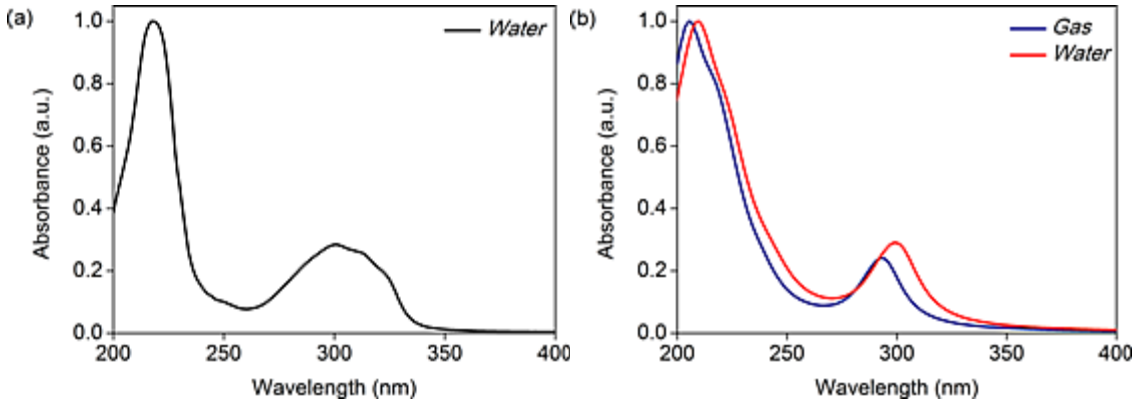

Figure 4.8 (a) Experimental and (b) Theoretical spectra of Q8C.

Table 4.14 Experimental and theoretical values for Q8C.

Experimental	Calculated			
Water	Water			
λ (nm)	λ (nm)	E (eV)	f	MO contribution
218	210	5.90	0.61	HOMO-4→LUMO HOMO-1→LUMO+2
300	300	4.13	0.23	HOMO-1→LUMO,HOMO-2→LUMO
	Gas			
	205	6.05	0.40	
	293	4.23	0.15	

4.3 FRONTIER MOLECULAR ORBITALS (FMOs)

The frontier molecular orbitals (FMOs) are the highest occupied molecular orbital (HOMO) and lowest unoccupied molecular orbital (LUMO) and are the most important orbitals in molecule [75]. These orbitals are termed as frontier as they lie at the outer most boundaries of the electrons of the molecules [76]. Many properties of molecules such as chemical reactivity, kinetic stability and site of electrophilic attack can be understood fully through HOMO-LUMO analysis [75]. The energy of the HOMO is directly related to the ionisation potential *I* and LUMO energy is directly related to the electron affinity *A* as given by the Koopman's theory [77]

$$-\varepsilon_{HOMO} = I \text{ and } -\varepsilon_{LUMO} = A \quad (4.1)$$

Energy difference between HOMO and LUMO orbitals known as energy gap is an important parameter in determining chemical stability of a molecule [78]. Wider HOMO-LUMO gap means harder and less reactive molecule whereas narrower HOMO-LUMO gap indicates softer and more reactive molecule [77,82,83]. By using the HOMO and LUMO energy values, the global chemical reactivity indices given by the following relations [77, 79-83]

$$Electronegativity\ \chi = \frac{(I+A)}{2} \quad (4.2)$$

$$Chemical\ hardness\ \eta = \frac{(I-A)}{2} \quad (4.3)$$

$$Chemical\ potential\ \mu = -\chi \quad (4.4)$$

$$Electrophilicity\ index\ \omega = \frac{\mu^2}{2\eta} \quad (4.5)$$

were calculated for both gas and solvent (water) phase. The results are presented in Table 4.15.

In general, 3D plots of the key frontier orbitals around HOMO and LUMO of the tittle molecules are qualitatively similar with each other and therefore only plots for Q2C is reported in Figure 4.9. The 3D plots demonstrated that the FMOs are dominated by π and π* orbitals, therefore the electronic transitions can be assingned as π→π* transitions. This is expected because the molecules have a lot of π bonds. However, there is no significant relation between these HOMO and LUMO energies quantities and λ_{max} shifts with the change in position of carboxaldehyde moiety, which are already quite small.

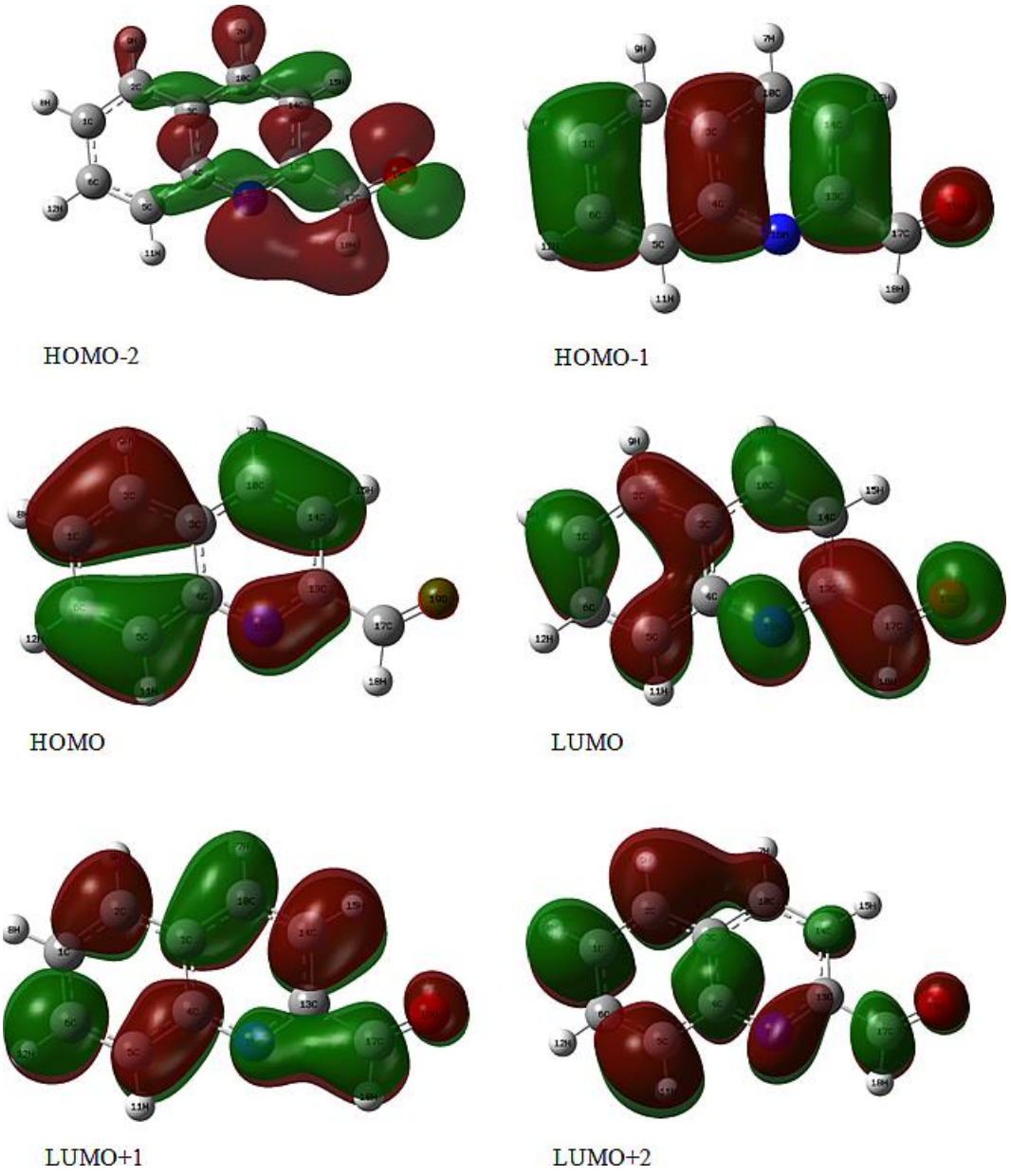

Figure 4.9 FMOs for Q2C.

Table 4.15 Global electrophilicity indices for QC derivatives.

		E_{tot} (E_H)	$E_{LUMO}+2$	$E_{LUMO}+1$	E_{LUMO}	E_{HOMO}	E_{HOMO-1}	E_{HOMO-2}	E_{HOMO-4}	E_{HOMO-5}	ΔE^a	η	χ	μ	ω
Q2C	Gas	-515.265092	-0.49	-1.74	-2.62	-7.02	-7.32				-4.40	2.20	4.82	-4.82	5.27
	Water	-515.274553	-0.33	-1.61	-2.64	-6.84	-7.37				-4.20	2.1	4.74	-4.74	5.34
Q3C	Gas	-515.263024	-0.55	-1.68	-2.72	-7.03	-7.33				-4.30	2.15	4.87	-4.87	5.52
	Water	-515.273121	-0.38	-1.56	-2.64	-6.87	-7.44				-4.23	2.12	4.75	-4.75	5.33
Q4C	Gas	-515.263681	-0.95	-1.22	-2.89	-6.95	-7.40		-8.88		-4.05	2.03	4.90	-4.92	5.97
	Water	-515.275871	-0.88	-1.10	-2.83	-6.88	-7.35		-8.82		-4.05	2.02	4.86	-4.86	5.83
Q5C	Gas	-515.259274	-1.22	-1.54	-2.68	-7.07	-7.27	-7.56		-9.84	-4.39	2.20	4.87	-4.87	5.40
	Water	-515.270677	-1.05	-1.42	-2.60	6.96	-7.34	-7.39		-9.75	-4.36	2.18	4.78	-4.78	5.24
Q6C	Gas	-515.256593	-0.59	1.85	-2.54	-7.12	-7.45		-9.05		-4.58	2.29	4.83	-4.83	5.10
	Water	-515.267542	-0.41	-1.73	-2.44	-6.96	-7.40		-8.85		-4.52	2.26	4.70	-4.70	4.88
Q7C	Gas	-515.25924	-0.66	-1.67	-2.64	-7.04	-7.38		-9.00		-4.40	2.20	4.84	-4.84	5.32
	Water	-515.27067	-0.53	-1.52	-2.60	-6.90	-7.42		-8.83		-4.30	2.15	4.75	-4.75	5.25
Q8C	Gas	-515.268262	-1.05		-2.51	-6.62	-7.06	-7.51	-8.83		-4.11	2.06	4.56	-4.56	5.06
	Water	-515.279183	-0.96		-2.47	-6.88	-6.98	-7.36	-8.76		-4.41	2.26	4.73	-4.73	4.94

[a] $\Delta E = E_{HOMO} - E_{LUMO}$. *All quantities are in eV except* E_{tot} *which is in Hartree.*

4.4 MOLECULAR ELECTROSTATIC POTENTIAL (MESP)

Molecular electrostatic potential of a molecule is the net electrostatic effect, produced by the total charge distribution (electrons and nuclei) of the molecule. MESP is mainly used to predict the sites for electrophilic [84] and nucleophilic [85] attacks. MESP map depicts not only the site for reactivity but also the size and shape of a molecule as well as electron charge distribution [85,86]. The MESP of the title molecules have been plotted with the same basis set of 6-311++G(d,p). The MESP plots are again similar with each other and only plot of Q2C is presented in Figure 4.10. The colours in the MESP map correspond to different values of potential. Potential increases in the order red<orange<yellow<green<blue. Red, the low-energy end of the scale is used for the regions of the most negative electrostatic potential, blue is used to colour regions of the most positive electrostatic potential [78] while, green colour indicates neutral electrostatic potential region [84,85].

As can be seen from the MESP map, the regions having the negative electrostatic potential is mainly localised around the electronegative atoms; oxygen of carboxaldehyde group and nitrogen of pyridine ring. These atoms can be predicted as possible sites of electrophilic attack. Oxygen atom is found to have more concentration of charge than nitrogen atom. Therefore electrophile specie will attack QC prefarencially at oxygen and nitrogen atoms positions. Positive potential is found around all the hydrogen atoms thus, predicting sites for nucleophilic activities. Neutral region is found around the carbon atoms of the aromatic ring predicting dormacy in chemical activity.

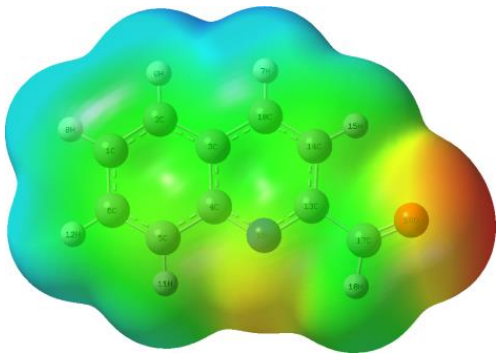

Figure 4.10 MESP for Q2C.

CHAPTER 5

CONCLUSION

In the current contribution, the experimental and theoretical electronic absorption spectra of QC derivatives were studied. Theoretical calculations were using DFT performed at B3LYP/6311++G(d,p) level. Conformational properties of the molecules, geometric parameters (bond length and bond angle), FMOs and MESP analyses for the tittle molecules were also presented. QC exhibits two different conformers depending on the orientation of CHO which we called as Rot1 and Rot2. Theoretical calculations showed Rot1 to be more stable and therefore all computational results of it were reported.

Theoretical spectra were simulated in gas phase and in water solvent. Absorption maxima for lower-lying singlet states were calculated by TD-DFT/B3LYP/6-311++G(d,p). The absorption bands were observed to show slight red-shift in the present of solvent. Analysis of the molecular orbitals shows that the absorption maxima of these molecules correspond to electon transitons between FMOs such as HOMO to LUMO and so on. Plots of FMOs show that the FMOs are mainly composed of π and π^* orbitals and thus electronic transitions are designated as $\pi \rightarrow \pi^*$.

The experimental spectra were recorded in the range of 190-1100 nm with the aid of UV-vis spectrophometer. Comparisons of the experimental and theoretical spectra show very good agreement. Hence TD-DFT proves to be powerful computational tool for investigation of electronic absorption spectra. MESP plot indicates oxygen and nitrogen as sites for electrophilic attack whereas hydrogen atoms as sites of nucleophilic attack.

REFERENCES

[1] Jones, G., (editor), *Chemistry of Hetrocyclic Compounds*, Vol. 32, John Wiley, New York, 1977.

[2] Jia, C.S., Zhang, Z., Tu, S.J. and Wang, G.W., "Rapid and Efficient Synthesis of Poly-substituted Quinolines Assisted by p-toluene Sulphonic Acid Under Solvent-free Conditions: Comparative Study of Microwave Irradiation Versus Conventional Heating", *Org. Biomol. Chem*., pp. 104-110, 2006.

[3] Kannappan, N., Reddy, B.S.R., Sen, S., Nagarajan, R. and Dashputa, S., "Synthesis and Chemical Characterization of Quinoline Imine Derivatives" *J. Appl. Chem. Res*., Vol. 9, pp. 59-68, 2009.

[4] Scott, E.D. and Venkatraman, S., "On the Mechanism of the Skraup-Doebner-Von Miller Quinoline Synthesis", *J. Org. Chem*., Vol. 71, pp. 1668-1676, 2006.

[5] Abbott, J.A., Acheson, R.M., Forder, R.A., Watkin, D.J. and Carruthers, J.R., "Pentamethyl11,11a-Dihyfloro-9-oxo9H,10Hcyclobuta[4,5]cyclo-penta[3,4]pyrrolo[1,2a]quinoline7,8,10,11,11a-pentacarboxylate", *Acta Cryst.*, Vol. 32B, pp. 1927-1929, 1976.

[6] Finar, I.L., *Organic Chemistry*, Vol. 1, Longman, England, 1995.

[7] Linck, R., Ziegler, J. and Wright, D.W., "Heme Aggregation Inhibitors: Antimalarial Drugs Targeting an Essential Biomineralization Process", *Curr. Med. Chem.*, Vol. 8, pp. 171-189, 2001.

[8] Chauhan, P.M.S. and Srivastava, S.K., "Present Trends and Future Strategy in Chemotherapy of Malaria", *Curr. Med. Chem.,* Vol.8, pp. 1535-1542, 2001.

[9] Famin, O., Krugliak, M. and Ginsburg, H., **"**Kinetics of Inhibition of Glutathione-mediated Degradation of Ferriprotoporphyrin IX by Antimalarial Drugs*", Biochem. Pharmacol.*, Vol. 58**,** pp. 59-68, 1999.

[10] Ismail, F.M.D., Dascombe, M.J., Carr, P. and Merette, S.A.M., "Novel Aryl-Antimalarials with Antimalarial Activity in Vivo", *J. Pharm. Pharmacol.*, Vol. 50, pp. 483–492, 1998.

[11] Go, M.L., Ngiam, T.L., Tan, A.L.C., Kuaha, K. and Wilairat, P., "Structure-activity Relationships of Some Indolo[3,2-*c*]quinolines with Antimarial Activity", *Eur. J. Pharm. Sci*., Vol. 6, pp.19-26, 1998.

[12] Dorn, A., Vippagunda, S.R., Mitile, H., Jaquet, C., Vennerstrom, J.L. and Ridley, R.G., "An Assessment of Drug-Haematin Binding as a Mechanism for Inhibition of Haematin Polymerisation by Quinoline Antimalarials", *Biochem. Pharmcol*., Vol. 55, pp. 727-736, 1998.

[13] Egan, T.J., Ross, D.C. and Adams, P.A., "Quinoline Anti-malarial Drugs Inhibit Spontaneous Formation of p-haematin (Malaria Pigment)", *FEBS Lett*., Vol. 352, pp. 54-57, 1994.

[14] Kuroda, Y., Ogawa, M., Nasu, H., Jerashima, M., Kasahara, M., Kiyama, Y., Wakita, M., Fujiwara, Y., Fujii, N. and Nakagawa, J., "Locations of Local Anesthetic Dibucaine in Model Membranes and the Interaction Between Dibucaine and a Na^+ Channel Inactivation Gate Peptide as Studied by ^{2}H-and ^{1}H-NMR Spectroscopies", *Biophys. J.*, Vol. 71, pp. 1191-1207, 1996.

[15] Dube, D. et al, "Quinolines as Potent 5-lipoxygenase Inhibitors: Synthesis and Biological Profile of L-746,530", *Bioorg. Med. Chem. Lett*., Vol. 8, pp. 1255-1260, 1998.

[16] Gupta, R., Gupta, A.K., Paul, S. and Kachroo, P.L. "Synthesis and Biological Activities of Some 2-chloro-6/8-substituted-3-(3-alkyl/aryl-5,6-dihydro-s-triazolo[3,4-b][1,3,4]thiadiazol-6-yl)quinolines," *Ind. J. Chem.,* Vol. 37B, pp. 1211–1213, 1998.

[17] Gupta, R., Gupta, A.K., Paul, S. and Somal, P., "Microwave-assisted Synthesis and Biological Activities of Some 7/9-substituted-4-(3-alky Varyl-5,6-Dihydro-s-triazolo[3,4-b][1,3,4] thiadiazol-6-yi)-tetrazolo[1,5-a]quinolines", *Ind. J. Chem.*, pp. 847-852, 2000.

[18] Mistry, B.D., Desai, K.R., Patel, J.A. and Patel N.I., "Conventional and Microwave-assisted Synthesis of Pyrazole Derivatives and Screening of their Antibacterial and Antifungal Activities", *Ind. J. Chem.,* Vol. 51B, pp.746-751, 2012.

[19] Kidwai, M., Bhushan, K.R., Sapra, P., Saxena R.K. and Gupta, R. "Alumina-supported Synthesis of Antibacterial Quinolines using Microwaves", *Bioorg. Med. Chem. Lett.*, Vol. 8, pp. 69-72, 2000.

[20] Tiwari, S., Chauran, P.M.S. and Bhaduri, D.P, "Syntheses and Antifilarial Profile of 7-Chloro-4-(substituted Amino) Quinolines: a New Class of Antifilarial Agents", *Bioorg. Med. Chem. Lett*., Vol. 10, pp. 1409, 2000.

[21] Nayyar, A., Malde, A., Coutinho, E. and Jain, R., "Synthesis, Anti-tuberculosis Activity, and 3D-QSAR Study of Ring-substituted-2/4 Quinolinecarbaldehyde Derivatives*" Bioorg. Med. Chem.*, Vol.14, pp. 727, 2006.

[22] Edwards, J.P., West, S.J., Marschke, K.B., Mais, D.E., Gottardis, M.M. and Jones, T.K., "5-Aryl-1,2-dihydro-5H-chromeno-[3,4-f]quinolines as Potent, Orally Active, Nonsteroidal Progesterone Receptor Agonists: The Effect of D-Ring Substituents", *J. Med. Chem.*, Vol. 41, pp. 303-310, 1998.

[23] Coghlan, M.J., Kym, P.R. and Elmore, S.W., "Synthesis and Characterization of Non-Steroidal Ligands for the Glucocorticoid Receptor: Selective Quinoline Derivatives with Prednisolone-Equivalent Functional Activity", *J. Med. Chem.* Vol. 44, pp. 2879-2885, 2001.

[24] Hamann, L.G., Higuchi, R.I., Zhi L., Edwards, J.P., Wang, X.N., Marschke, K.B., Kong, J.W., Farmer, L.J. and Jones, T.K., "Synthesis and Biological Activity of a Novel Series of Nonsteroidal, Peripherally Selective Androgen Receptor Antagonists Derived from 1,2-Dihydropyridono[5,6-g]quinolines", *J. Med. Chem*., Vol. 41, pp. 623-639, 1998.

[25] Edwards, J.P., Higuchi, R.I., Winn, D.T., Pooley, C.L., Caferro, T.R., Hamann, L.G., Zhi, L., Marschke, K.B., Goldman, M.E. and Jones, T.K., "Nonsteroidal Androgen Receptor Agonists Based on 4-(trifluoromethyl)-2H-pyrano[3,2-g]quinolin-2-one", *Bioorg. Med. Chem. Lett*., Vol. 9, pp. 1003–1008, 1999.

[26] Zhi, L., Tegley, C.M., Kallel, E.A., Marschke, K.B., Mais, D.E., Gottardis, M.M. and Jones, T.K., "5-Aryl-1,2-dihydrochromeno[3,4-*f*]quinolines: A Novel Class of Nonsteroidal Human Progesterone Receptor Agonists", *J. Med. Chem.*, Vol. 41, pp. 291-302.

[27] Marella, A., Tanwar, O.P., Saha, R., Ali, M.R., Srivastava, S., Akhter, M., Shaquiquzzaman, M. and Alam, M.M., "Quinoline: A Versatile Heterocyclic", *Saudi Pharm. J.*, Vol. 21, pp. 1-12, 2012.

[28] Deady, L.W., Desneves, J., Kaye, A.J., Finlay, G.J., Baguley, B.C. and Denny, W.A., "Positioning of the Carboxamide Side Chain in 11-Oxo-11H-indeno[1,2-b]quinolinecarboxamide Anticancer Agents: Effects on Cytotoxicity", *Bioorg. Med. Chem.*, Vol. 9, pp. 445-452, 2001.

[29] Nomland, A. and Hills, I.D., "2-Quinolinecarboxaldehyde: an Unusual Partner in the Henry Reaction and Subsequent Elimination", *Tetrahedron Lett.,* Vol. 9, pp. 5511-5514, 2008.

[30] Rosenberg, E., Rokhsana, D., Nervi, C., Gobetto, R., Milone, L., Viale, A., Fiedler, J. and Botavina, M.A., "Synthesis, Reduction Chemistry, and Spectroscopic and Computational Studies of Isomeric Quinolinecarboxaldehyde Triosmium Clusters", *Organometallics*, Vol. 23, pp. 215-223, 2004.

[31] Chen, Z.F., Zhang P., Xiong, R.G., Liu, D. and You, X.Z., "The First One-dimensional Metal–Organic Coordination Polymer with 4-quinolineacarboxylate as Building Block: $[Cd(\mu_2\text{-}H_2O)(4\text{-quinolinecarboxylato-}O,O]_2$", *Inorg. Chem. Commun.*, Vol. 5, pp. 35–37, 2002.

[32] Tsotinis, A. et al, "A Facile Synthesis of C2-Substituted Pyrrolo[2,3-f]quinolines with Cytotoxic Activity", *Lett. in Drugs Design and Discov*., Vol. 2, pp. 189-192, 2005.

[33] Albinati, A., Anklin, C.G., Ganazzoli, F., Ruegg, H. and Pregosin, P.S., "Preparative and ^1H NMR Spectroscopic Studies on Palladium(I1) and Platinum(I1) Quinoline-8-carbaldehyde (1) Complexes. X-ray Structures of the Cyclometalated Acyl Complex $PdCl(C(O)C_9H_6N)(PPh_3)\cdot PPh_3$ and *trans* - $PtCl_2(1\ )(PEt_3)$", *Inorg. Chem.*, Vol. 26, pp. 503-508, 1987.

[34] Talrose, V., Stern, E.B., Goncharova, A.A., Messineva, N.A., Trusova, N.V. and Efimkina, M.V., "UV/Visible Spectra", in Linstrom, P.J. and Mallard, W.G. (Eds.), *NIST Chemistry WebBook, NIST Standard Reference Database Number 69***,** National Institute of Standards and Technology, Gaithersburg MD, 20899, http://webbook.nist.gov

[35] Ozel, A.E., Buyukmurat, Y. and Akyuz, S., "Infrared-spectra and Normal-coordinate Analysis of Quinoline and Quinoline Complexes", *J. Mol. Struct.*, Vol. 565-566, pp. 455-462, 2001.

[36] Kucuk, V., Altun, A. and Kumru, M., "Combined Experimental and Theoretical Studies on the Vibrational Spectra of 2-quinolinecarboxaldehyde", *Spectrochim. Acta 85A*, pp. 92-98, 2012.

[37] Kumru, M., Kucuk, V. and Bardakci, T., "Theoretical and Experimental Studies on the Vibrational Spectra of 3-quinolinecarboxaldehyde", *Spectrochim. Acta 90A*, pp. 28-34, 2012.

[38] Kumru, M., Kucuk, V. and Kocademir, M., "Determination of Structural and Vibrational Properties of 6-quinolinecarboxaldehyde using FT-IR, FT-Raman and Dispersive-Raman Experimental Techniques and Theoretical HF and DFT (B3LYP) methods", *Spectrochim. Acta 96A*, pp. 242-251, 2012.

[39] Kumru, M., Kucuk, V. and Akyurek, P., "Vibrational spectra of quinoline-4-carbaldehyde: Combined Experimental and Theoretical Studies", *Spectrochim. Acta 113A*, pp. 72–79, 2013.

[40] Peckson, R.L., Shields, L.D., Cairns, T. and McWilliam, I.G., *Modern Methods of Chemical Analysis*, 2nd edition, John Wiley, New York, 1968.

[41] Beeson, S. and Mayer, J.W., *Patterns of Light, Chasing the Spectrum from Aristotle to LEDs*, Springer Science+Business Media, New York, 2008.

[42] Skoog, D.A., Hooler, F.J. and Crouch, S.R., *Principles of Instrumental Analysis*, 6th edition, Thomson Brooks/Cole, Canada, 2007.

[43] Streetman, B.G. and Banerjee, S.K., *Solid Electronic Devices*, 6th edition, PHI Learning Private Limited, New Delhi, 2009.

[44] Pavia, D.L., Lampman, G.M., Kriz G.S. and Vyvyan, J.R., *Introduction to Spectroscopy*, Brooks/Cole Cangage Learning, USA, 2009.

[45] Rao, C.N.R., *Ultraviolet and Visible Spectroscopy Chemical Application*, London Butter Worths, 1961.

[46] Braun, R.D., *Introduction to Instrumental Analysis*, McGraw-Hill, Singapore, 1987.

[47] Crooks, J.E., *The Spectrum in Chemistry*, Academic Press, London, 1978.

[48] McQuarrie, D.A., *Quantum Chemistry*, University Science Books, USA, 1983.

[49] Hollas, J.M., *Basic Atomic and Molecular Spectroscopy*, Royal Society of Chemistry, UK, 2002.

[50] Levine, I.N., *Molecular Spectroscopy*, John Wiley, Canada, 1975.

[51] Hollas, J.M., *Modern Spectroscopy*, 4th edition, John Wiley, England, 2004.

[52] Banwell, C.N., *Fundamental of Molecular Spectroscopy*, 3rd edition, Mc Graw-Hill, England, 1983.

[53] Perdew, J.P. and Kurth, S., *Density Functional Theory for Non-relativistic Coulomb Systems in the New Century*, Springer-Verlag, Berlin Heidelberg, 2005.

[54] Atkins, P. and Friedman, R., *Molecular Quantum Mechanics*, 4th edition, Oxford University Press, 2005.

[55] Lewars, E.G., *Computational Chemistry*, 2nd edition, Springer Dordrecht, Heidelberg, 2011.

[56] Mueller, M., *Fundamentals of Quantum Chemistry*, Kluwer Academic Publishers, New York, 2002.

[57] Parr, R.G. and Yang, W., *Density Functional Theory of Atoms and Molecules*, Oxford University Press, 1989.

[58] Koch, W. and Holthausen, M.C., *Chemist's Guide to Density Functional Theory,* 2nd edition, Wiley-VCH Verlag GmbH, Germany, 2001.

[59] Sholl, D.S. and Steckel, J.A., *Density Functional Theory*, John Wiley, Canada, 2009.

[60] Jensen, F., *Introduction to Computational Chemistry*, 2nd edition, John Wiley, England, 2007.

[61] M.J. Frisch, G.W. Trucks, H.B. Schlegel, G.E. Scuseria, M.A. Robb, J.R. Cheeseman, J.A. Montgomery Jr., T. Vreven, K.N. Kudin, J.C. Burant, J.M. Millam, S.S. Iyengar, J. Tomasi, V. Barone, B. Mennucci, M. Cossi, G. Scalmani, N. Rega, G.A. Petersson, H. Nakatsuji, M. Hada, M. Ehara, K. Toyota, R. Fukuda, J. Hasegawa, M. Ishida, T. Nakajima, Y. Honda, O. Kitao, H. Nakai, M. Klene, X. Li, J.E. Knox, H.P. Hratchian, J.B. Cross, V. Bakken, C. Adamo, J. Jaramillo, R. Gomperts, R. E. Stratmann, O. Yazyev, A.J. Austin, R. Cammi, C. Pomelli, J.W. Ochterski, P.Y. Ayala, K. Morokuma, G.A. Voth, P. Salvador, J.J. Dannenberg, V.G. Zakrzewski, S. Dapprich, A.D. Daniels, M.C. Strain, O. Farkas, D.K. Malick, A.D. Rabuck, K. Raghavachari, J.B. Foresman, J.V. Ortiz, Q. Cui, A.G. Baboul, S. Clifford, J. Cioslowski, B.B. Stefanov, G. Liu, A. Liashenko, P. Piskorz, I. Komaromi, R.L. Martin, D.J. Fox, T. Keith, M.A. Al-Laham, C.Y. Peng, A. Nanayakkara, M. Challacombe, P.M.W. Gill, B. Johnson, W. Chen, M.W. Wong, C. Gonzalez, J.A. Pople, Gaussian 03, Revision C.02, 2004, Gaussian, Inc., Wallingford, CT, 2004.

[62] Nielsen A. B. and Holder A.J., *Gauss View 5.0, User's Reference*, GAUSSIAN Inc., Pittsburgh, PA, 2009.

[63] Briquet, L., Varcauteren, D.P., Andre, J.M., Perpete, E.A. and Jacquemin, D., "On the Geometries and UV/Vis Spectra of Substituted Trans-azobenzenes", *Chem. Phys. Lett*., Vol. 435, pp. 257-262, 2007.

[64] Ok, S., Altun, A., Kasimogullari, R. and San, E., "Role of the H‑Bond Interactions in the Colloidal Mixtures of Pyrazole-Based Bioactive Dyes and Poly(vinyl alcohol)", *J. Chem. Eng. Data*, Vol. 58, pp. 3521-3527, 2013.

[65] Jacquemin, D., Perpete, E.A., Sclalmani, G., Frisch, M.J., Ciofini, I. and Adamo, C., "Absorption and Emission Spectra in Gas-phase and Solution using TD-DFT: Formaldehyde and Benzene as Case Studies", *Chem. Phys. Lett*., Vol. 421, pp. 272-276, 2006.

[66] Preat, J., Loos, P.F., Assfeld, X., Jacquemin, D. and Perpete, E.A., "A TD-DFT Investigation of UV Spectra of Pyranoidic Dyes: A NCM vs PCM Comparison", *J. Mol. Struct*., Vol. 808, pp. 85-91, 2007.

[67] Tomasi, J., Mennucci, B. and Cances, E., *J. Mol. Struct.:THERMO*, "The IEF Version of the PCM Solvation Method: An Overview of a New Method Addressed to Study Molecular Solutes at the QM *Ab Initio* Level", Vol. 464, pp. 211-226, 1999.

[68] Jacquemin, D., Assfeld, X. and Perpete, E.A., "Solvent Effects on the Geometry and First Hyperpolarizability of Polymethineimine", *J. Mol. Struct.*, Vol. 710, pp.13-17, 2004.

[69] Rouessae, F. and Rouessae, A., *Chemical Analysis*, 2nd edition, John Wiley, England, 2007.

[70] Robinson, J. W., Frame, E.M.S. and Frame, G.M., *Undergraduate Instrumental Analysis*, 6th edition, Marcel Dekker, 2005.

[71] Settle, F. (editor), *Handbook of Instrumental Techniques for Analytical Chemistry*, Prentice Hall, USA, 1997.

[72] Altun, A., Golcuk, K. and Kumru, M., "Theoretical and Experimental Studies of the Vibrational Spectra of m-methylaniline", *J. Mol. Struct.*, Vol. 625, pp. 17-24, 2003.

[73] Karabacak, M., Kose, E. and Karaca, C., "Spectroscopic (NMR, UV, Ft-IR and FT-Raman) Analysis and Theoretical Investigation of Nicotinamide N-oxide With Density Functional Theory", *Spectrochim. Acta 83A*, pp. 250-258, 2011.

[74] Grimme, S., "Calculation of the Electronic Spectra of Large Molecules", in Lipkowitz, K.B., Larter, R. and Cundari, T.R. (Eds.), *Reviews in Computational Chemistry*, Vol. 20, pp. 153-211, John Wiley, USA, 2004.

[75] Fleming, I., *Frontier Orbitals and Organic Chemical Reactions*, John Wiley, Chichester, 1976.

[76] Muthu, S., Rajamani, T., Karabacak, M. and Asiri, A.M., "Vibrational and UV Spectra, First-order Hyperpolarizability, NBO and HOMO-LUMO analysis of 4-chloro-N-(2-methyl-2,3-dihydroindol-1-yl)-3-sulfamoyl-benzamide", *Spectrochim. Acta*, Vol. 122, pp. 1-14, 2014.

[77] Pearson, R.G., "Absolute Electronegativity and Hardness Correlated with Molecular Orbital Theory", *Proc. Natl. Acad. Sci. USA*, Vol. 83, pp. 8440-8441, 1986.

[78] Govindarajan, M. and Karabacak, M., "Spectroscopic Properties, NLO, HOMO–LUMO and NBO Analysis of 2,5-Lutidine", *Spectrochim. Acta 96A*, pp. 421-435, 2012.

[79] Pearson, R.G., "Chemical Hardness and Bond Dissociation Energies", *J. Am. Chem. Soc.* Vol. 110, pp. 7684-7690, 1988.

[80] Pearson, R.G., *J. Am. Chem. Soc*. "Ionization Potentials and Electron Affinities in Aqueous Solution", Vol. 108, pp. 6109-6114, 1986.

[81] Pearson R.G., "Absolute Electronegativity and Absolute Hardness of Lewis Acids and Bases", *J. Am. Chem. Soc*., Vol. 107, pp. 6801-6806, 1985.

[82] Mebi, C.A., "DFT Study on Structure, Electronic Properties, and Reactivity of *cis*-isomers of $[(NC_5H_4\text{-}S)_2Fe(CO)_2]$", *J. Chem. Sci.,* Vol. 123, pp. 727-731, 2011.

[83] Parr, R.G., and Yang, W., *Density Functional Theory of Atoms and Molecules*, Oxford University Press, 1989.

[84] Joshi, B.D., Srivastava A., Honorato, S.B., Tandon, P., Pessao, O.D.L., Fechine, P.B.A. and Ayala, A.P., "Study of Molecular Structure, Vibrational, Electronic and NMR Spectra of Oncocalyxone A using DFT and Quantum Chemical Calculations", *Spectrochim. Acta 113A*, pp. 367–377, 2013.

[85] Xavier, R.J. and Dinesh, P., "Spectroscopic (FTIR, FT-Raman, ^{13}C and ^{1}H NMR) Investigation, Molecular Electrostatic Potential, Polarizability and First-order Hyperpolarizability, FMO and NBO Analysis of 1-methyl-2-imidazolethiol", *Spectrochim. Acta 118A*, pp. 999–1011, 2014.

[86] Petrucci, H., Herring, F.G., Madura, J.D., and Bissonnette, C., *General Chemistry*, 10^{th} edition, Pearson, Canada, 2011.